East Pye Solar DCO - Written Representation

Interested Party reference: [redacted]

Summary of Written Representation

The Scheme's claimed carbon benefit is central to the planning balance. I identify significant uncertainties in the calculation, timing and resilience of that benefit which I have not found to be resolved in the Applicant's assessment.

I identify apparent errors, inconsistencies and uncertainties in the Applicant's lifecycle carbon calculations, including PV manufacturing emissions, and the absence of a stated carbon payback period. I question the counterfactual used for the 60-year carbon saving and the absence of sensitivity analysis of key assumptions.

I identify a lack of evidence demonstrating resilience to severe but plausible weather, in particular the wind/storm severity and return period the infrastructure is designed to withstand and how events beyond that basis have been considered, when even a nominal 1-in-87-year event has approximately a 50% probability of occurring at least once over 60 years.

Finally, the Scheme’s proximity to other proposed large-scale solar developments creates potential correlated exposure to severe regional weather, simultaneous loss of generating capacity and constrained recovery resources. I have not identified an assessment of this geographic concentration risk. Taken together, the material before the ExA does not establish the robustness of the claimed long-term carbon benefit or adequately justify the proposed concentration of further substantial generating capacity in this location.

Written Representation

1. I am an Interested Party and a local resident. I recognise the compelling need for clean energy and the contribution it can make to a safer and more sustainable world for future generations. In my Relevant Representation I raised the substantial adverse effects of the Scheme and questioned whether the application had adequately addressed the full lifecycle carbon impacts of construction, maintenance, replacement and decommissioning.

2. At the Procedural Meeting on 15 September I raised the importance of demonstrable rigour in the carbon case. The Applicant referred me to the Statement of Need [APP-206] and Planning Statement [APP-209]. Having further considered those and other relevant application documents, this Written Representation develops the lifecycle carbon concern raised in my Relevant Representation.

3. If local environmental, agricultural and amenity impacts are to be accepted in return for long-term public benefits, there should be sufficient confidence that those benefits will materialise and be sustained over the proposed 60-year operational life, and that risks to their delivery are appropriately mitigated through siting, design, management and operation.

4. My representation is informed by over 30 years' experience as a finance professional within the insurance industry and considers matters relevant to the robustness and deliverability of the claimed long-term benefits.

Basis of the PV and replacement carbon estimates

5. The Applicant estimates construction emissions of 347,673 tCO2e, including 87,445 tCO2e for PV arrays and mounting structures [APP/6.1.6, Table 6.25]. The estimate is based on constituent material carbon factors.

6. A recent peer-reviewed lifecycle assessment reports cradle-to-gate emissions of 412 kgCO2e/kWp for bifacial PERC modules manufactured in China using the national-average electricity mix.[1] The Applicant

assumes that the Scheme's panels will be sourced from China [APP/6.1.6, para 6.9.60]. On an illustrative 500 MWp, the study's factor would indicate approximately 206,000 tCO2e for module manufacture. By comparison, the Applicant's constituent-material calculation produces approximately 85,000 tCO2e for the panels when its stated glass inputs are applied arithmetically (see 7 below). The Applicant uses a product-level manufacturing emissions factor for BESS. This raises a question as to whether the calculation approach captures the full manufacturing carbon footprint of the PV arrays.

7. Two of the stated calculations also appear not to reconcile with their underlying inputs.

Glass — paragraph 6.9.16
Applicant's inputs: 26,393 tonnes × 1.4028 kgCO_2e/kg
Calculated result: approximately 37,024 tCO_2e
Reported result: 1,371 tCO_2e

Mounting structures — paragraphs 6.9.18–6.9.19
Applicant's inputs: 9,973 structures × 800 kg × 2.71 kgCO_2e/kg
Calculated result: approximately 21,621 tCO_2e
Reported result: 37,845 tCO_2e

Correcting both figures using the Applicant's stated inputs increases the combined PV-and-mounting estimate from 87,445 tCO_2e to approximately 106,870 tCO_2e.

8. Finally, I have not seen figures for the end-of-life emissions associated with PV panels and BESS equipment removed and replaced during the operational life of the Scheme, as distinct from equipment remaining in place until final decommissioning.

Testing the 60-year carbon benefit forecast against severe but plausible adverse experience

9. I use 'return period' to refer to infrequent but potentially severe events. It expresses the annual probability of an event of a particular severity; for a given type of event, a longer return period will generally correspond to a more severe event. The Applicant itself uses this approach for flood risk: Chapter 4 specifies the elevation of electrical infrastructure by reference to the 1-in-100-year flood level [APP/6.1.4, para 4.3.17 and Table 4.1].[2]

10. Over 60 years, severe weather events with relatively long return periods cannot reasonably be treated as remote. Assuming a constant annual probability, a 1-in-20-year event has approximately a 95% probability of occurring at least once over 60 years. Even a 1-in-87-year event has a 50% probability - it is as likely as not.[3]

11. The Applicant's Planning Statement records national policy requiring the physical impacts of climate change to be considered when planning the location, design, construction and operation of new energy infrastructure, and states that Chapter 6 sets out the Scheme's resilience to climate change [APP-209, paras 8.2.77-8.2.81].[17]

12. The Applicant says the Scheme has considered resilience to extreme weather and that panels and infrastructure will withstand high winds in accordance with relevant standards and guidance [APP/5.11, p.189]. It also states that extreme-weather risks and resilience to climatic change over the 60-year life have been considered [APP/6.1.6, para 6.5.49], and recognises that projected climate changes and environmental extremes are likely to become more severe during operation [para 6.9.149]. However, I have not identified the severe-weather conditions against which that resilience was assessed, in particular the wind or storm severity and expected return period the PV panels and their mounting structures are required to withstand, or how events exceeding that design basis have been considered.[4] For context, Kettle (2023) records that Storm Kyrill's wind speeds in Germany were assessed at the level of a 50-year return-period event; the storm caused widespread infrastructure damage and disruption across Europe.[5]

13. The CCRA assigns increased storm intensity a Very Low likelihood and Minor adverse consequence [APP/6.1.6, Table 6.37]. The Applicant states that consequence ratings use professional judgement and supporting evidence,[6] but I have not identified the supporting evidence for that rating or the nature, severity and probability of the storm event being assessed in relation to the PV panels and their mounting structures. Experience from insured weather losses also illustrates the uncertainty associated with estimating the

frequency of severe events from historical experience. Swiss Re found that a French hail event-loss level previously associated with a 20–50-year market return period had been exceeded three times within a decade, requiring reconsideration of industry return-period assumptions; using the additional data, it estimated the return period at less than ten years. Swiss Re also notes that climate change could influence the intensity and frequency of convective storms, although current trends remain highly uncertain.[7]

14. A 2025 IEA-PVPS review records structural wind damage to fixed-tilt and single-axis tracker systems, including cases where winds below typical or project design speeds caused damage, with consequences including lost generation, repowering, shipping, recycling and disposal costs.[8] These also are relevant to the Applicant's assumption that mounting structures will not require replacement [APP/6.1.6, para 6.9.76].

15. Chapter 6 also identifies ‘deterioration of structures or foundations due to decrease in soil moisture levels’ as a potential operational climate risk [APP/6.1.6, Table 6.37]. However, the measure identified in the assessment for lower summer rainfall concerns provision of stored water for fire suppression.[6]

16. The Ground Conditions Assessment identifies potential land-instability and subsidence risks and records clay strata and former clay pits within or adjoining parts of the selected site. [9] The wider South Norfolk area is also characterised by substantial clay geology. Chapter 4 provides for piled mounting structures up to 4 m deep [APP/6.1.4, Table 4.1], but I have not identified evidence demonstrating how the depth and design of those foundations address shrink-swell ground movement from prolonged dry periods. BGS identifies shrink-swell ground movement as a significant geohazard and expects warmer, drier summers and increased rainfall variability to increase shrink-swell activity. This is particularly relevant to the suitability and resilience of the site selected for infrastructure intended to operate for 60 years.[9]

17. Recent UK experience also indicates increasing exposure to drought-related subsidence. Subsidence surge years occurred in 2018, 2022 and 2025, associated with prolonged hot and dry conditions and soil-moisture deficit.[10]

18. The evidence before the ExA therefore leaves material uncertainty as to the Scheme's resilience to severe weather over its 60-year operating life, and consequently as to the suitability of the selected site for infrastructure intended to operate for that period.

The magnitude and timing of the carbon benefit depend on Scheme performance and underlying assumptions

19. The Applicant estimates a lifetime operational carbon saving of approximately 1.3 MtCO2e, against its figure of approximately 0.35 MtCO2e of construction emissions incurred before operation [11] (subject to the calculation issues identified at paragraph 7 above). I have not identified a calculation showing when that initial carbon outlay is offset by operational carbon savings (the carbon payback period).

20. The claimed saving is sensitive to the counterfactual. Chapter 6 describes the comparator both as the 'forecast UK Grid Average' [para 6.4.31] and as 'long-run marginal grid emissions forecasts for 2031' [para 6.7.5]. The basis of the comparator therefore requires clarification. The lifespan saving is calculated using the 2031 grid emissions factor, although, on the NESO pathways the Applicant cites, rapid subsequent decarbonisation follows, reaching zero or below by around 2035.[12] Applying a 2031 comparator across a 60-year life may therefore overstate the emissions that would otherwise occur and is too simplistic a basis for a claimed carbon benefit of such importance to the planning balance.

21. The comparison is also more complex than a single grid factor suggests. Average grid factors do not capture all whole-life emissions of the generation mix, and the emissions actually avoided by solar may depend on the marginal generation displaced.

22. These factors can operate in different directions, reinforcing the need for sensitivity testing. I have not identified analysis showing the effect on the claimed 1.3 MtCO2e saving of alternative grid-decarbonisation assumptions, marginal generation or later commencement. The material before the ExA therefore does not establish the robustness of the headline saving.

23. In my professional experience of reviewing long-term financial and capital assessments, sensitivity analysis is essential where projections depend on assumptions extending over a long period (here 60 years). Here this could test the effect on lifetime carbon benefit and payback of severe weather-related

damage, premature replacement and uncertainty in decommissioning emissions, alongside the counterfactual sensitivities identified above.

Physical and financial resilience are relevant to the durability of the claimed benefits

Physical resilience

24. Chapter 6 states that climate projections and asset sensitivities were reviewed to identify appropriate resilience measures [APP/6.1.6, para 6.9.143]. However, I have not identified testing of severe-but-plausible scenarios to compare alternative sites, layouts or design choices, including their consequences for damage, recovery, lost generation and carbon benefit. Such analysis could inform the suitability of the selected site relative to alternatives, as well as the way the Scheme is designed and operated - for example, the choice between fixed and tracking panels - rather than serving only as a test of its overall carbon case.

25. Lost generation is a permanent loss of carbon benefit, while repair or premature replacement may add embodied carbon, construction traffic and local impacts. Measures that avoid or limit damage and enable rapid reinstatement therefore protect the long-term benefits relied upon.

Financial resilience

26. Financial resilience is relevant to prompt repair or reinstatement after a severe loss. Insurance can transfer some financial risk, but sufficient resources are also required for uninsured costs and recovery. I have not identified an assessment of the financial consequences of a severe operational loss, or evidence of the financial and insurance arrangements supporting recovery.

Geographic concentration creates an additional resilience- and energy-security risk

27. The Scheme would not operate in geographic isolation. The Applicant records High Grove and The Droves at 31 km and 41 km respectively from the Order Limits. Together, the three proposed large-scale solar installations represent approximately 1.72 GW of generating capacity.[13]

28. A severe regional weather event could affect more than one installation simultaneously due to their proximity. Research into European windstorms has examined 'extreme-tail dependence' – the tendency for extreme events to occur at more than one location. For pairs of locations less than 50 km apart, 69% of those studied showed results statistically consistent with such dependence, compared with only 3% for pairs 150–200 km apart.[14] This supports considering the three nearby schemes as potentially exposed to a common severe regional wind event. Simultaneous impairment of a substantial concentration of generation is relevant to national energy-system resilience and security.

29. Concentration could also exacerbate recovery through simultaneous demand for replacement equipment, specialist contractors and network repair capacity. Swiss Re identifies geographic concentration, shared infrastructure and specialist suppliers as sources of correlated loss, and notes that supply-chain bottlenecks and extended replacement times can increase the cost of recovery.[15] US Solar Fund plc states that it uses geographic diversification across its solar portfolio to reduce exposure to any one extreme-weather or environmental event.[16]

30. I have not identified an Applicant assessment of either the risk of simultaneous impairment of generating capacity contributing to national energy security or the additional recovery risk concentration could create for the Scheme. Without a fully supported assessment of these risks and their mitigation, such a concentration of substantial generating capacity in this location is not adequately justified.

Overall

31. Taken together, these matters create material uncertainty over the scale, timing and resilience of the carbon benefit relied upon over the Scheme's 60-year life. They are also relevant to whether the selected site, in an area of substantial geographic concentration, is appropriate for large-scale solar generation and whether different siting, design or operational choices could reduce those risks. The local environmental, landscape, agricultural and amenity impacts arise from development of this particular site. The material

before the ExA should therefore provide sufficient confidence that the long-term carbon benefit relied upon to justify those impacts is robust and that the proposed location does not expose its delivery to avoidable risk.

Use of Artificial Intelligence

32. I have used OpenAI ChatGPT to assist me in searching and navigating the Applicant's extensive documentation, identifying relevant passages and external sources, analysing and organising the issues considered in this representation, and assisting with drafting and editing. I have reviewed the resulting analysis and source references, and the observations and conclusions expressed in this representation are my own. I take responsibility for the material submitted.

References

[1] Yuan, L., Farina, A. and Anctil, A. (2024), 'How will manufacturing capacity additions in China and North America affect the carbon footprint of silicon photovoltaics?', Sustainable Production and Consumption, 49, 236-248. DOI: 10.1016/j.spc.2024.06.014. Publicly available through the US National Science Foundation Public Access Repository. Accessed 6 October 2026.

[2] East Pye Solar, Environmental Statement Volume 1, Chapter 4 - The Scheme [APP/6.1.4], para 4.3.17 and Table 4.1.

[3] Arithmetic: for constant annual probability 1/R, probability of at least one occurrence in 60 years = 1 - (1 - 1/R)^60.

[4] East Pye Solar, Consultation Report Appendix 10, Section 47 Applicant Response Table [APP/5.11], p.189; Environmental Statement Volume 1, Chapter 6 - Climate Change [APP/6.1.6], paras 6.5.49 and 6.9.149.

[5] Kettle, A.J. (2023), 'Storm Kyrill and the storms of mid-January 2007: Societal and Energy Impacts in Europe', Advances in Geosciences, 58, 135-147, Section 5 (Conclusion). Accessed 6 October 2026. Exhibit 01.

[6] East Pye Solar, Environmental Statement Volume 1, Chapter 6 - Climate Change [APP/6.1.6], including para 6.5.54 and Table 6.37.

[7] Swiss Re, 'Severe 2022 hail damage in France sets new benchmarks, underscores shift of risk and calls for pricing adjustments' (2022), 'Resetting event loss benchmarks'. Accessed 6 October 2026.

[8] IEA Photovoltaic Power Systems Programme (IEA-PVPS), Task 13, Operational and Economic Impacts of Extreme Weather on PV Power Plants, Report IEA-PVPS T13-33:2025 (December 2025), relevant extracts at pp.9-10 and 16-19. Exhibit 03.

[9] East Pye Solar, Environmental Statement Volume 3, Appendix 16.1 - Phase 1 Ground Conditions Assessment [APP/6.3.16.1]; East Pye Solar, Environmental Statement Volume 1, Chapter 4 - The Scheme [APP/6.1.4], Table 4.1; British Geological Survey, GeoClimate: shrink-swell, accessed 6 October 2026. Exhibit 04.

[10] Milliman (20 August 2026), 'UK property insurance subsidence event: A 2026 reserving update'. Accessed 6 October 2026.

[11] East Pye Solar, Environmental Statement Volume 1, Chapter 6 - Climate Change [APP/6.1.6], Table 6.25, para 6.9.63 and para 6.9.117.

[12] East Pye Solar, Environmental Statement Volume 1, Chapter 6 - Climate Change [APP/6.1.6], paras 6.4.31, 6.7.5 and 6.9.117; Statement of Need [APP-206], paras 5.2.13-5.2.14.

[13] East Pye Solar, Environmental Statement Volume 3, Appendix 2.4 - Cumulative Schemes (High Grove approximately 31 km; The Droves approximately 41 km); scheme capacity information.

[14] Dawkins, L.C. and Stephenson, D.B. (2018), 'Quantification of extremal dependence in spatial natural hazard footprints: independence of windstorm gust speeds and its impact on aggregate losses', Natural Hazards and Earth System Sciences, 18, 2933-2949, section 3.2, p.2940. Accessed 6 October 2026. Exhibit 02.

[15] Swiss Re Institute, sigma 3/2026, Time to build: expanding the frontier of insurability for the capex super-cycle, Chapter 3, 'More correlated and concentrated insurance risks'. Accessed 6 October 2026.

[16] US Solar Fund plc, Annual Report and Financial Statements 2024, Task Force on Climate-related Financial Disclosures, p.38. Accessed 6 October 2026.

[17] East Pye Solar, Planning Statement [APP-209], paras 8.2.77-8.2.81 (physical climate-change impacts, adaptation and resilience).

What is shrink–swell?

Many soils contain clay minerals that absorb water when wet (making them swell) and lose water as they dry (making them shrink). This 'shrink–swell' behaviour is controlled by the type and amount of clay in the soil and by changes in soil-moisture content related to rainfall and local drainage. This shrink–swell variation can cause ground movement, which in turn may damage building foundations, pipes or utility services.

How does climate change affect shrink–swell?

Dry weather and high temperatures are a major factor in the emergence of subsidence in clay soils. Every summer can be completely different to the last; summer 2018 had the hottest, driest June for years whereas summer 2019 had one of the wettest Junes on record. Warmer, drier summers and increases in annual temperature and rainfall variability are predicted, which will cause more shrink–swell activity.

What is the impact of shrink–swell?

Shrink–swell ground movement, typically reported as subsidence, is one of the most damaging geohazards in Britain today, costing the economy an estimated £3 billion over the past decade. It can lead to financial loss for anyone involved in the construction, ownership or management of property, large structures, infrastructure networks and utilities. These costs could include increased insurance premiums, depressed house prices and, in some cases, engineering works to stabilise land or property.
Armed with knowledge about potential hazards, preventative or mitigative steps can be put in place to alleviate the effects of the hazard on property and infrastructure. The cost of such prevention may be very low and is often many times lower than the repair bill following ground movement

Further information

GeoClimate looks specifically at the geological factors that influence shrink–swell subsidence and the climatic effects and interactions. It does not consider any human or artificial factors. GeoClimate shrink–swell provides information on the potential for clay shrink–swell subsidence under a range of climate scenarios. The data provides projections for the RCPs 2.6, 4.5 and 8.5 emission scenarios.

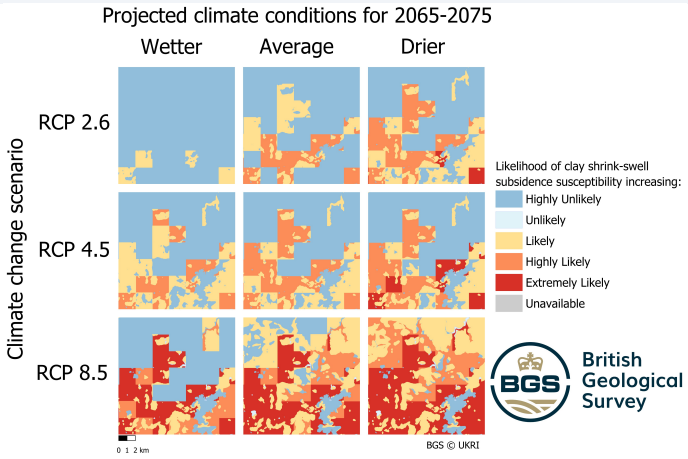

Matrix of sample BGS GeoClimate clay shrink–swell outputs for the wettest, average and driest projected climate conditions in each of the RCPs 2.6, 4.5 and 8.5, for the time period of 2065 to 2075. BGS © UKRI

Nat. Hazards Earth Syst. Sci., 18, 2933–2949, 2018
[redacted]
© Author(s) 2018. This work is distributed under
the Creative Commons Attribution 4.0 License.

Natural Hazards and Earth System Sciences
Open Access

Quantification of extremal dependence in spatial natural hazard footprints: independence of windstorm gust speeds and its impact on aggregate losses

[redacted]
College of Engineering, Mathematics and Physical Sciences, University of Exeter, Exeter, UK

Correspondence: [redacted]

Received: 7 April 2018 – Discussion started: 23 April 2018
Revised: 22 October 2018 – Accepted: 23 October 2018 – Published: 8 November 2018

Abstract. Natural hazards, such as European windstorms, have widespread effects that result in insured losses at multiple locations throughout a continent. Multivariate extreme-value statistical models for such environmental phenomena must therefore accommodate very high dimensional spatial data, as well as correctly representing dependence in the extremes to ensure accurate estimation of these losses. Ideally one would employ a flexible model, able to characterise all forms of extremal dependence. However, such models are restricted to a few dozen dimensions, hence an a priori diagnostic approach must be used to identify the dominant form of extremal dependence.

Here, we present various approaches for exploring the dominant extremal dependence class in very high dimensional spatial hazard fields: tail dependency measures, copula fits, and conceptual loss distributions. These approaches are illustrated by application to a data set of high-dimensional historical European windstorm footprints (6103 spatial maps of 3-day maximum gust speeds at 14 872 locations). We find there is little evidence of asymptotic extremal dependency in windstorm footprints. Furthermore, empirical extremal properties and conceptual losses are shown to be well reproduced using Gaussian copulas but not by extremally dependent models such as Gumbel copulas. It is conjectured that the lack of asymptotic dependence is a generic property of turbulent flows. These results open up the possibility of using geostatistical Gaussian process models for fast simulation of windstorm hazard fields.

1 Introduction

Multivariate statistical models are increasingly used to explore the spatial characteristics of natural hazard footprints and quantify potential aggregate losses. For example, such models for European windstorms are used by academics and (re)insurers to create catalogues of possible events, explore loss potentials, and benchmark synthetic events from atmospheric models (Bonazzi et al., 2012; Youngman and Stephenson, 2016).

Natural hazards, such as European windstorms, have widespread effects, often causing insured losses at many locations throughout a continent. Therefore, statistical models for such hazards must accommodate very high dimensional data in order to represent the full hazard domain. Moreover, since natural hazards are rare events in the tail of the distribution, these statistical models must also correctly represent the dependence in the extremes to ensure valid inference and, hence, a realistic representation of the hazard's aggregate losses.

When modelling multivariate extremes, variables can be described as being either *asymptotically dependent*, where large values of the variables tend to occur simultaneously, or *asymptotically independent*, where the largest values rarely occur together (Coles et al., 1999). As noted by Wadsworth et al. (2017), examples of modelling joint extremes often assume asymptotic dependence in order to accommodate asymptotically justified extreme-value max-stable models, which can potentially lead to overestimation of the joint occurrences of extremes. The assumption of asymptotic dependence is common in the field of natural hazard research.

Coles and Walshaw (1994) used a max-stable model for the dependence in maximum wind speeds in different directions, Blanchet et al. (2009) to model snow fall in the Swiss Alps, Huser and Davison (2013) to model extreme rainfall, and Bonazzi et al. (2012) to model windstorm hazard fields at pairs of locations in Europe. Indeed, Bonazzi et al. (2012) simply base this modelling assumption on being "in line with many examples found in the literature". However, it is important to question this assumption of asymptotic dependence.

Two approaches are used for exploring, and correctly representing, extremal asymptotic dependence. Either one can estimate the dependence by fitting a suitably flexible extreme-value model capable of representing dependence and independence, or alternatively one can perform diagnostic tests to identify the dependence class, i.e. whether or not extremal dependence is present.

There is a growing literature in the area of flexible models for extremal dependence, originating from the bivariate tail model of Ledford and Tawn (1996). Wadsworth and Tawn (2012) developed a spatial model, involving inverted max-stable and max-stable models, able to incorporate both forms of extremal dependence. This model, however, requires the estimation of a large number of parameters and is only able to transition between dependence classes at a boundary point of the parameter space. Following this, Wadsworth et al. (2017) explored more flexible transitions between extremal dependence classes and developed a model able to represent a wider variety of dependence structures, although limited to the bivariate case. Huser et al. (2017) went on to develop a flexible extension of the Wadsworth et al. (2017) model using Gaussian scale mixtures, in which the two asymptotic dependence regimes are smoothly blended. As noted by Huser and Wadsworth (2018), however, this model either makes the transition between dependence class at a boundary point of the parameter space (as in Wadsworth and Tawn, 2012) or is inflexible in its representation of the asymptotic independence structure. Most recently, Huser and Wadsworth (2018) presented a flexible model able to provide a smooth transition between both extremal dependence classes using only a small number of parameters.

While these models provide advantages in terms of flexibility and are growing in their applicability to higher dimensions, none are computationally feasible yet for very high dimensional data sets (Huser and Wadsworth, 2018). For example, max-stable models for asymptotic dependence are limited in application to a few dozen variables due to the computational demand of existing fitting methods (de Fondeville and Davison, 2018). Hence, as noted by Huser and Wadsworth (2018), with the exception of the specific high-dimensional peaks-over-threshold model of de Fondeville and Davison (2018), truly high-dimensional inference for spatial extreme-value models has yet to be achieved.

Therefore, when aiming to model very high dimensional data, the alternative, a priori identification approach must be taken. Several studies have developed and/or employed diagnostic measures to identify the form of extremal dependence between variables. Ledford and Tawn (1996, 1997) developed a bivariate tail model in which one of the parameters, named the coefficient of tail dependence, is used within a diagnostic approach to help identify the bivariate extremal dependence class. Coles et al. (1999) introduced two extremal dependence coefficients, $\chi(p)$ and $\overline{\chi}(p)$, characterising the conditional probability of a pair of locations exceeding the same high quantile threshold $1-p$, for which the asymptotic limit (as $p \to 0$) provides a diagnostic of bivariate extremal dependence. Bortot et al. (2000) used pairwise scatter plots and empirical estimates of $\chi(p)$ and $\overline{\chi}(p)$ to diagnose the form of extremal dependence present in a three-dimensional data set of sea surge, wave height, and wave period in South West England. They found evidence for asymptotic independence and hence developed a multivariate Gaussian tail model for their data, derived from the joint tail of a multivariate Gaussian distribution with margins based on univariate extreme-value distributions. Similarly, Eastoe et al. (2013) applied the coefficient of tail dependence, the χ and $\overline{\chi}$ measures, and the conditional extremes model of Heffernan and Tawn (2004) to estimate the form of extremal dependence in 3 hourly sea surface elevation maxima at 15 locations, identifying, in general, asymptotic dependence. Similarly, more recently, Kereszturi et al. (2015) employed the coefficient of tail dependence and χ and $\overline{\chi}$ measures within a comprehensive theoretical framework to assess extremal dependence of North Sea storm severity along four strips of 14 locations within the North Sea.

In all of the above examples these diagnostic approaches are applied to a relatively small number of locations. Here we present an approach for systematically exploring the dominant form of extremal dependence within a high-dimensional natural hazard data set. Specifically, we demonstrate this approach using a large (6103 events) and very high dimensional data set (14 872 locations) of climate-model-generated European windstorm footprints.

We introduce the bivariate diagnostic measures of Ledford and Tawn (1996) and Coles (2001) in the context of our approach by initially using them to explore the bivariate extremal dependence in two pairs of locations within the European domain (London–Amsterdam and London–Madrid) and subsequently present an approach for systematically applying the same diagnostics throughout the high-dimensional domain. We use the simple extremal dependence measures of Ledford and Tawn (1996) and Coles (2001) as they are quick to compute and can therefore be calculated for many thousands of pairs of locations, which is important when exploring very high dimensional data.

In addition, we contribute a further diagnostic, relevant for natural hazard modelling, by presenting an approach for exploring the impact of extremal dependence misspecification on conceptual aggregate hazard loss estimation. We use the Gaussian and Gumbel copula models, representing asymptotic independence and dependence respectively, to

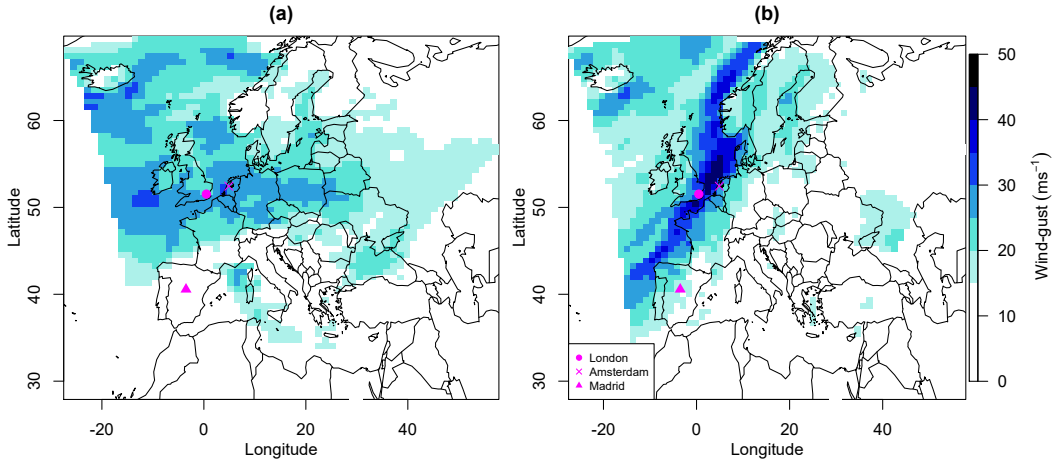

Figure 1. Hazard footprints for windstorms **(a)** Kyrill and **(b)** the Great Storm of October 1987, with the location of the cities of London, Amsterdam, and Madrid indicated.

model pairs of locations, and quantify the discrepancy between modelled and observed joint conceptual losses. This approach is introduced for one central location, paired with all other locations in the high-dimensional domain, and then extended to systematically explore the full domain. The approaches presented in this paper can be used to explore extremal dependence and develop appropriate multivariate statistical models for other high-dimensional natural hazard data sets.

Section 2 describes the windstorm hazard data set used throughout this paper. Section 3 introduces and applies the extremal dependence diagnostics of Ledford and Tawn (1996) and Coles et al. (1999), initially to two pairs of locations and then to systematically explore the high-dimensional data domain. Section 4 demonstrates how extremal dependence influences conceptual aggregate losses. Section 5 presents ideas from turbulence theory for why wind gust speeds are likely to be asymptotically independent, and, finally, Sect. 6 concludes.

2 Data

The windstorm footprint data set used in this study is the same as that used in Dawkins et al. (2016) and an extended version of the data set used in Roberts et al. (2014), consisting of the 6103 high-resolution model-generated windstorm footprints, for windstorm events that occurred within the European domain during the 35 extended winters (October–March) 1979/1980–2013/2014 (kindly provided by Jessica J. Standen and Julia F. Lockwood at the Met Office).

The windstorm footprint is defined as the maximum 3 s wind gust speed (in metres per second) at grid points in the region 35 to 70° N in latitude and 15° W to 25° E in longitude and over a 72 h period centred on the time at which the maximum 925 hPa wind speed occurred over land. The 925 hPa wind speed is taken from ERA-Interim reanalysis (Dee et al., 2011). The 3 s wind gust speed has a robust relationship with storm damage (Klawa and Ulbrich, 2003) and is commonly used in catastrophe models for risk quantification (Roberts et al., 2014). A 72 h windstorm duration is commonly used in the insurance industry (Haylock, 2011) and is thought to capture the most damaging phase of the windstorm (Roberts et al., 2014).

These 6103 historical windstorm events have been identified using the objective tracking approach of Hodges (1995), and the associated footprints are created by dynamically downscaling ERA-Interim reanalysis to a horizontal resolution of 25 km using the Met Office Unified Model (MetUM). As described by Roberts et al. (2014), the wind gust speeds are calculated from wind speeds in the MetUM model, based on a simple gust parameterisation, $U_{\mathrm{gust}} = U_{10\,\mathrm{m}} + C\sigma$, where $U_{10\,\mathrm{m}}$ is the wind speed at 10 m altitude and σ is the standard deviation of the horizontal wind, estimated from the friction velocity using the similarity relation of Panofsky et al. (1977). The roughness constant C is determined from the universal turbulence spectra and is larger over rough terrain.

The MetUM-generated footprints for Kyrill (17–19 January 2007) and the Great Storm of October 1987 (15–17 October 1987) are shown in Fig. 1. The variability in the intensity and location of extreme, damaging winds in these footprints demonstrates the potential importance of correctly modelling the spatial dependence between locations for realistically representing joint losses.

Using model-generated windstorm footprints for representing historical storms has benefit in terms of spatial and temporal coverage; however these estimated maximum wind gust speeds will differ from those observed at nearby weather stations. For example, as noted by Roberts et al. (2014), several alternative methods for parameterising wind gust speeds

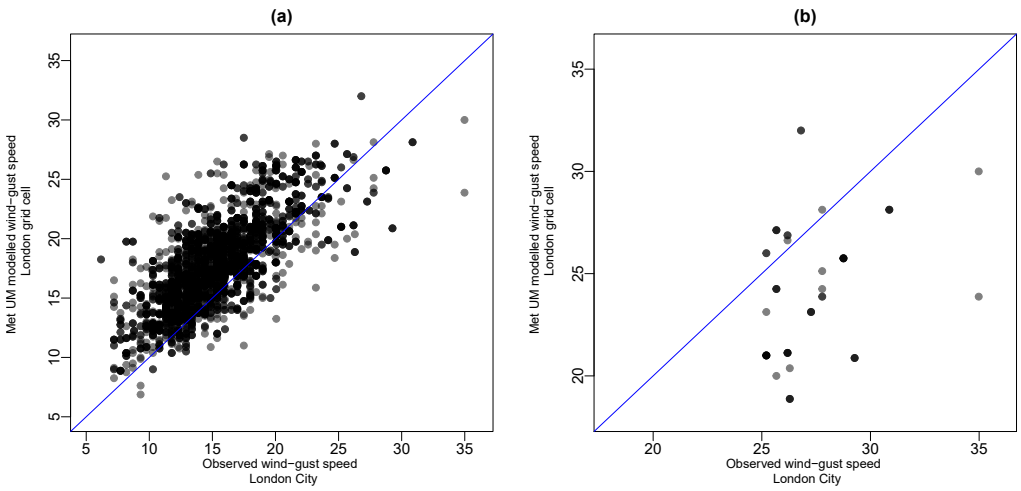

Figure 2. (a) The relationship between MetUM windstorm footprint wind gust speeds in the London grid cell and the corresponding observed wind gust speeds at the London City Airport weather station within the Global Summary of the Day data set, and **(b)** the same relationship for the 50 most extreme windstorm events at the London City Airport weather station. In both plots the line $y = x$ has been added for reference (blue).

are available (see Sheridan, 2011, for a review), which can lead to large differences in estimated gusts (10–20 m s^{-1}). The validity of simplistic gust parameterisation stated above was evaluated by Roberts et al. (2014), who found an overestimation in the effect of surface roughness at stations greater than $\sim$ 500 m altitude, leading to an underestimation in MetUM-modelled extreme winds in these locations. In addition, Roberts et al. (2014) identified a slight underestimation in extreme wind gust speeds greater than $\sim$ 25 m s^{-1}. This was found to be due to a number of mechanisms, including the underestimation of convective effects and strong pressure gradients, leading to the underdevelopment of fast-moving storms (Roberts et al., 2014).

To explore the possible discrepancy in the MetUM wind gust speed data relevant for this study, we extract daily maximum observed wind gust speed recorded at the London City Airport weather station (the station located within the London grid cell used throughout this study) from the Global Summary of the Day (GSOD) data repository and, for each of the 6103 windstorm events in our data set, find the maximum hourly observed gust in the 3-day period centred on the same date as in the MetUM-generated footprints. A comparison of the observed and MetUM-modelled footprint wind gusts in London is presented in Fig. 2a, indicating a general overestimation in modelled wind gust speeds below 25 m^{-1} and a slight underestimation for wind gust speeds above 25 m^{-1}, reflecting the findings of Roberts et al. (2014). Figure 2b presents this same relationship for the 50 most extreme events in the observed data set, highlighting this underestimation of modelled extreme wind gust speeds. Indeed, the root-mean-squared difference between the observed and modelled footprint wind gust speeds for these 50 extreme events is 4.57 m s^{-1}, which provides an estimate of the uncertainty in representing observed extreme windstorm gust speeds.

This discrepancy in model-generated wind gust speeds could lead to differences in results, namely the identification of the extremal dependence class between locations. To explore this possibility, we repeat the empirical analysis in Sect. 3 (Fig. 4) for GSOD data at London City Airport and Amsterdam Airport Schiphol, shown in Fig. S1 in the Supplement. We find that for this pair of locations the weather station and MetUM data have very similar relationships in the extremes, with the weather station data being slightly less dependent, therefore not changing the conclusions of this study.

3 Extremal dependency

As a motivating example, the bivariate dependence in windstorm footprint wind gust speeds for London paired with Amsterdam and Madrid is presented in Fig. 3a and c respectively. These three locations are shown in Fig. 1, and these two pairings are chosen because of their contrasting separation distances and hence degrees of dependence (as shown in Fig. S2). These scatter plots show a greater degree of dependence between London and Amsterdam compared to London and Madrid. Indeed, multiple windstorms have losses occurring in London and Amsterdam at the same time, where loss is associated with wind gust speeds exceeding the 0.99th quantile at a given location, characterised by the top right-hand corner of each plot in Fig. 3. However, does this level of dependence between London and Amsterdam necessarily suggest asymptotic dependence?

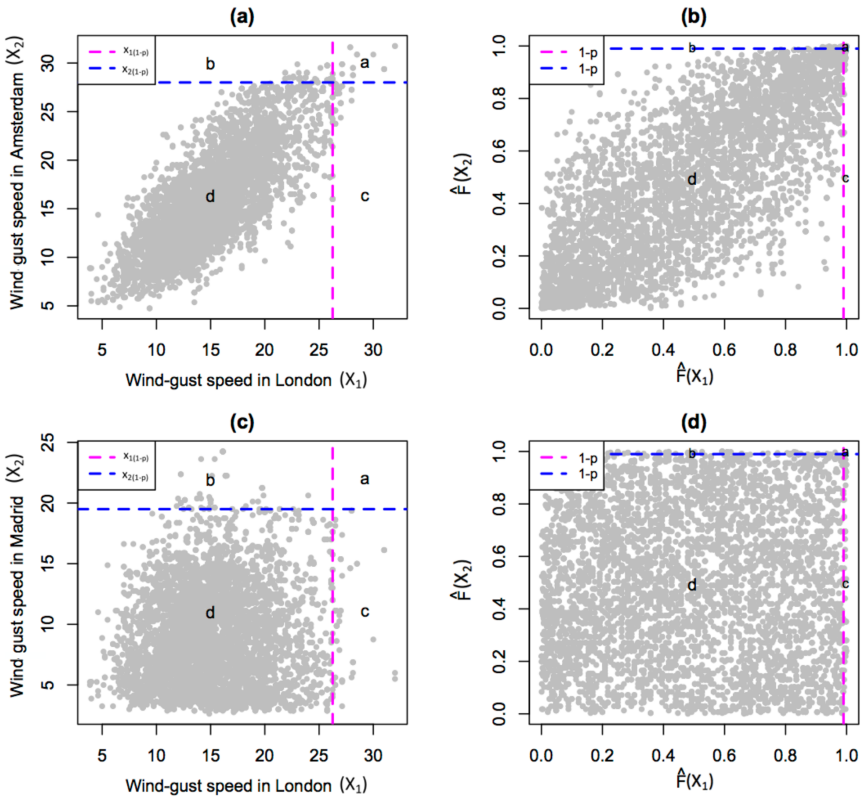

Figure 3. Scatter plot comparing historical windstorm footprint wind gust speeds ($\mathrm{m\,s^{-1}}$) in London with those in **(a)** Amsterdam and **(c)** Madrid, and empirical copula plots for London paired with **(b)** Amsterdam and **(d)** Madrid. Dashed lines show the 0.99th quantile of wind gust speed at each location, and labels a–d represent the number of points in each section of each plot, related to being above or below these high quantile thresholds.

The wind gust speeds at any two locations can be represented by the $n \times 2$ pair of random variables (X_1, X_2), where $n = 6103$ is the number of observations at each location. The joint distribution $Pr(X_1 \leq x_1,\ X_2 \leq x_2)$ is determined by the marginal distributions of each variable (i.e. $F_{X_1}(x_1) = Pr(X_1 \leq x_1)$ and $F_{X_2}(x_2) = Pr(X_2 \leq x_2)$) and their joint dependence. It can be shown that $Pr(X_1 \leq x_1,\ X_2 \leq x_2) = C(F_{X_1}(x_1),\ F_{X_2}(x_2))$, where $C(.,.)$ is a bivariate function known as a *copula* (Nelson, 2006). In other words, the marginal distributions can be factored out by using the respective cumulative distribution functions to transform the variables into variables $(F_{X_1}(X_1),\ F_{X_2}(X_2))$ that have uniform distributions over the interval [0, 1]. A simple way to do this is to use the empirical cumulative distribution function $(\hat{F}_{X_j}(x) = \frac{1}{n}\sum_{i=1}^{n} 1_{X_{ji} \leq x})$. This empirical copula approach simply amounts to considering the respective ranks of the X_1 and X_2 values divided by the sample size as shown in Fig. 3b and d.

3.1 Diagnostic measures

The degree of conditional dependence between X_1 and X_2 at a specified high quantile threshold, $1-p$, can be explored, based on the empirical copula, using the extremal dependence measures, $\chi(p)$ and $\overline{\chi}(p)$, introduced by Coles et al. (1999). The asymptotic limit of these measures, as $p \to 0$, can then be used to classify the class of bivariate extremal dependence between X_1 and X_2 as either *asymptotically dependent* or *asymptotically independent*. These measures are defined as

$$\chi(p) = Pr\left(X_2 > x_{2(1-p)} | X_1 > x_{1(1-p)}\right) = \frac{Pr\left(X_2 > x_{2(1-p)}, X_1 > x_{1(1-p)}\right)}{p}, \quad (1)$$

where $x_{1(1-p)}$ and $x_{2(1-p)}$ are the $(1-p)$th quantiles of X_1 and X_2 respectively, $0 \leq \chi(p) < 1$ for all $0 \leq (1-p) \leq 1$, and

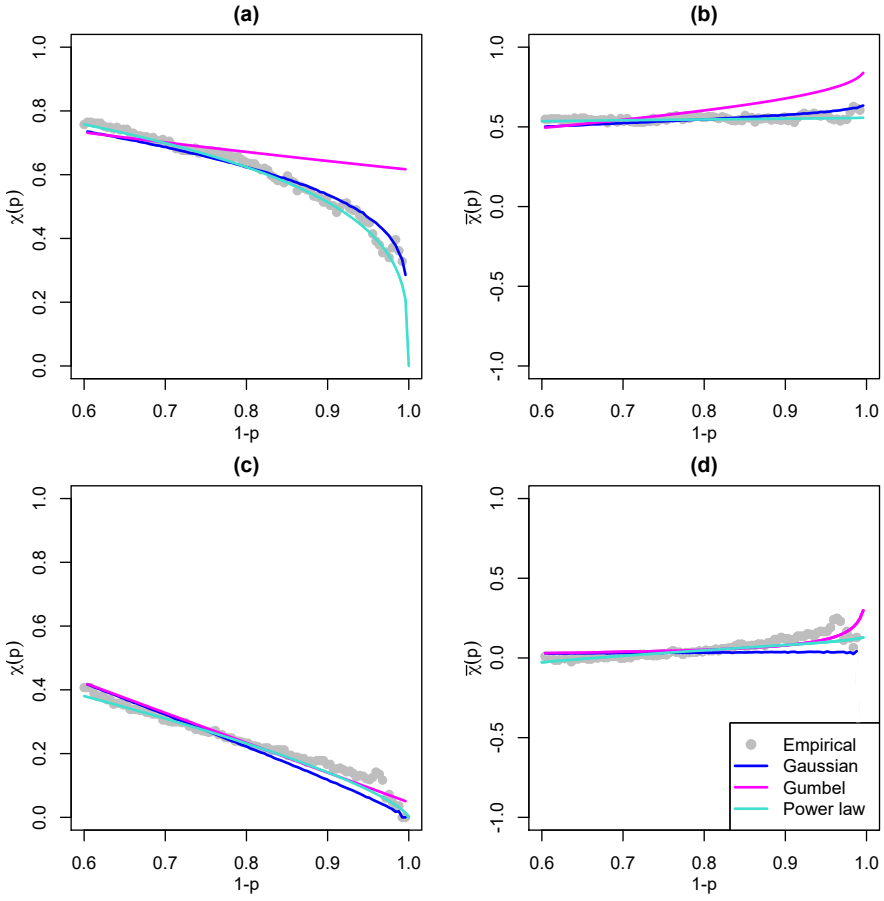

Figure 4. Extremal dependence measure $\chi(p)$, for $p \in [0, 0.4]$, for windstorm footprint wind gust speeds in London paired with **(a)** Amsterdam and **(c)** Madrid, and dependence measure $\overline{\chi}(p)$, for $p \in [0, 0.4]$, for windstorm footprint wind gust speeds in London paired with **(b)** Amsterdam and **(d)** Madrid, calculated empirically and based on the Gaussian, Gumbel, and power law bivariate dependence functions, as defined in Table A1.

$$\overline{\chi}(p) = \frac{2\log\left(Pr\left(X_1 > x_{1(1-p)}\right)\right)}{\log\left(Pr\left(X_1 > x_{1(1-p)}, X_2 > x_{2(1-p)}\right)\right)} - 1 = \frac{2\log(p)}{\log(\chi(p)p)} - 1 = \frac{\log(p) - \log(\chi(p))}{\log(p) + \log(\chi(p))}, \quad (2)$$

where $-1 \le \overline{\chi}(p) < 1$ for all $0 \le (1-p) \le 1$. Hence, if $\lim_{p\to 0}\chi(p) = \chi(0) > 0$, $\lim_{p\to 0}\overline{\chi}(p) = \overline{\chi}(0) = 1$, and the pair (X, Y) are said to be asymptotically dependent, with strength $\chi(0)$. If instead $\chi(0) = 0$, and hence $\overline{\chi}(0) < 1$, the pair are said to be asymptotically independent, and the non-vanishing measure $\overline{\chi}(0)$ represents the strength of this non-asymptotic dependence.

As an initial exploration of bivariate extremal dependence class between variables, these conditional probability measures can be calculated empirically over a range of quantile thresholds, as shown in Fig. 4 for windstorm footprint wind gust speeds in London paired with Amsterdam and Madrid. These empirical estimates are calculated as functions of the counts (a–d) in Fig. 3, as defined in Table A1. Based on these empirical estimates, for both pairs of locations, $\chi(p) \to 0$ and $\overline{\chi}(p) < 1$ as $p \to 0$, suggesting asymptotic independence.

However, here and as in all data sets of environmental phenomena, the rarity of very extreme events makes it impossible to empirically quantify the asymptotic limits $\chi(0)$ and $\overline{\chi}(0)$, necessary for extremal dependence class identification. To overcome this, Ledford and Tawn (1996) developed a bivariate tail model, able to characterise both classes of extremal dependence, which when fit to a bivariate random variable can be used to predict the asymptotic limit of the conditional probability measures and hence give an estimate of the class of extremal dependence, based on the sub-asymptotic evidence in the data and the assumption that the model can be extrapolated to asymptotic levels.

As in Ledford and Tawn (1996), let Z_1 and Z_2 denote X_1 and X_2 transformed to Fréchet margins respectively; that is, $Pr(Z_1 \le z) = Pr(Z_2 \le z) = \exp(-1/z)$. Then the joint

survivor function for Z_1 and Z_2 above some large quantile threshold z_{1-p} takes the form

$$Pr\left(Z_1 > z_{1-p}, Z_2 > z_{1-p}\right) \sim \mathcal{L}\left(z_{1-p}\right) p^{1/\eta}, \tag{3}$$

where $p = Pr(Z_1 > z_{1-p}) = Pr(Z_2 > z_{1-p})$, $\frac{1}{2} \leq \eta \leq 1$ is a constant and $\mathcal{L}(z_{1-p})$ is a slowly varying function as $p \to 0$. Based on this power law model, as shown by Coles et al. (1999),

$$\chi(p) \sim \mathcal{L}\left(z_{1-p}\right) p^{1/\eta - 1},$$

$$\overline{\chi}(p) = \frac{2\log(p)}{\log\left(\mathcal{L}\left(z_{1-p}\right)\right) + \frac{1}{\eta}\log(p)} - 1,$$
$$\to 2\eta - 1 \text{ as } p \to 0.$$

Hence, the parameter η, named the coefficient of tail dependence by Ledford and Tawn (1996), characterises the nature of the extremal dependence. When $\eta = 1$, $\chi(0) = \mathcal{L}(z_{1-p})$ and $\overline{\chi}(0) = 1$; hence the pair (X, Y) are asymptotically dependent on degree $\mathcal{L}(z_{1-p})$. Alternatively, if $\eta < 1$, $\chi(0) = 0$ and $\overline{\chi}(0) = 2\eta - 1$, and the pair are asymptotically independent with non-asymptotic dependence of degree $2\eta - 1$.

For a given pair, e.g. wind gust speeds in London and Amsterdam, the Ledford and Tawn (1996) model is fit to the joint survivor function along the diagonal, equivalent to the univariate distribution of $T = \min\{Z_1, Z_2\}$, known as the structure variable, which has length n. Using the stable two-parameter Poisson process representation of T presented by Ferro (2007), who employed the Ledford and Tawn (1996) model for the verification of extreme weather forecasts, the exceedance of T above a high threshold w has the form

$$Pr(T > t) = \frac{1}{n}\exp\left[-\left(\frac{t-\alpha}{\eta}\right)\right] \text{ for all } t \geq w, \tag{4}$$

with location parameter α and scale parameter $0 < \eta \leq 1$, equivalent to η in Eq. (3), estimated by maximum likelihood (Ferro, 2007).

Fitting this model to the pairs London–Amsterdam and London–Madrid requires the specification of the high threshold, w, above which the Poission process model is fit. As discussed by Ferro (2007), this threshold selection is a trade-off between being low enough that enough data are retained to ensure model precision, but high enough that the extreme-value theory that motivates the model provides accurate estimates. In a similar way to choosing the appropriate threshold when fitting a generalised Pareto distribution (see Coles, 2001), empirical diagnostic plots can be used to inform this selection. These include parameter stability plots, in which the estimated model parameters and mean excess should be constant above the chosen high threshold, and quality of fit plots, in which the transformed excesses, $(Z - w)/\eta$, should be exponentially distributed if an appropriately high threshold has been chosen (see Ferro, 2007, for more details).

Here, the 85 % quantile of the structural variable T is selected, based on these diagnostic plots (example for London–Amsterdam is presented in Fig. S3). This choice is similar to the 0.88 % and 0.9 % thresholds selected in the applications of Ferro (2007) and Ledford and Tawn (1996) respectively. Based on this choice of w, $\eta = 0.78 < 1$ for London–Amsterdam and $\eta = 0.58 < 1$ for London–Madrid, indicating asymptotic independence for both pairs of locations. This is further demonstrated in Fig. 4, which shows how the Ledford and Tawn (1996) model, referred to as the power law model, calculated as in Table A1, represents the conditional dependence measures $\chi(p)$ and $\overline{\chi}(p)$ as $p \to 0$, for London–Amsterdam and London–Madrid.

In addition, as a comparison (included in Fig. 4), alternative parametric bivariate dependence models known as the Gaussian and Gumbel copulas are used to model the pair (X_1, X_2) to give further indication of the extremal dependence class present.

The Gumbel bivariate copula model characterises asymptotic dependence with the degree of dependence quantified by parameter r. For each pair of locations, this parameter is estimated via maximum likelihood using the `copula` R package. The Gaussian bivariate model characterises asymptotic independence with dependence parameter ρ, here represented by the Spearman's rank correlation coefficient. Both models are fit to the full bivariate data pair, as presented in Fig. 3. For the Gumbel model the data are transformed to uniform margins using the empirical distribution function. The same transformation is made for the Gaussian model, followed by a transformation to Gaussian margins using the standard normal distribution function. The parametric forms of $\chi(p)$ and $\overline{\chi}(p)$ for these two opposing models are shown in Table A1. In Fig. 4, the Gumbel model is calculated as in Table A1; however, since the closed-form definition for the Gaussian model in Table A1 only holds for the limit $p \to 0$, for this model $\chi(p)$ and $\overline{\chi}(p)$ are estimated as the median of 1000 parametric bootstrap simulations from the associated bivariate normal distribution.

For both pairs of locations in Fig. 4, all three parametric bivariate dependence models indicate asymptotic independence. The power law model estimates $\chi(0) = 0$ and $\overline{\chi}(0) < 1$, the Gaussian model matches closely with the empirical estimates and the power law model, and the Gumbel model overestimates the conditional probability of joint extremes.

As a final diagnostic, analogous to that used by Ledford and Tawn (1996, 1997), the coefficient of tail dependence is estimated for a range of high thresholds, w, to explore the sensitivity of the parameter estimate to this choice. As in Ledford and Tawn (1996, 1997), here this diagnostic observes the proportion of time $\eta = 1$ is within the profile likelihood confidence interval for η, when estimated using w in the interval of the 0.5–1 quantile of T. The pair (X_1, X_2) are said to be asymptotically dependent if $\eta = 1$ is contained within these confidence intervals for a majority of the range

of w and asymptotically independent otherwise. This exploration is presented for London paired with Amsterdam and Madrid in Fig. 5, providing further evidence of asymptotic independence for both pairs, based on this criterion.

3.2 Extension to high dimensions

We now demonstrate a way of extending the quick-to-calculate coefficient of tail dependence diagnostic approach to systematically explore the dominant extremal dependence class across locations in a high-dimensional hazard field.

We first take a stratified (based on the distribution of locations over longitude and latitude) sample of 100 locations within the European domain. One such sample is shown in Fig. 6a. Since the extremal dependence is likely to decrease with increasing separation distance (Wadsworth and Tawn, 2012) and we hope to understand if asymptotic independence is dominant and hence present at small separation distances, for each of these 100 locations, we estimate the coefficient of tail dependence, η (and the associated 95 % profile likelihood confidence interval), when paired with the 100 nearest locations within the full domain. Figure 6b demonstrates how the 100 nearest locations are geographically distributed for one such sampled location in our windstorm footprint data set. For each pairing, the coefficient of tail dependence is calculated using w as the 0.9 quantile threshold of the structure variable, found to ensure stable estimates of η using diagnostic plots as in Fig. 6c. The estimated η parameters and confidence intervals for these 100×100 pairs of locations are plotted against separation distance to explore how, throughout the domain, η varies at small separation distances and changes with increasing separation distance, shown in Fig. 6d. The parameter estimate related to the pair of locations in pink and blue in Fig. 6b is shown in pink. This method is repeated many times with 10 such repetitions shown in Fig. S4, showing very similar results.

Figure 6d shows that for small separation distances ($<$ 180 km) a proportion of pairs of locations have coefficient of tail dependence parameters, η, close to 1, with $\eta = 1$ within the confidence interval indicating asymptotic dependence. Within the range (0–50 km) 69 % of pairs of locations exhibit this behaviour; however this proportion reduces rapidly as separation distance increases, to 30 % for locations separated by (50–100 km), 13 % for locations separated by (100–150 km), and 3 % for locations separated by (150–200 km). Hence, while there is evidence of asymptotic dependence for some locations in close proximity, even at very small separation distances (50 km) a larger proportion of locations exhibit asymptotic independence. Indeed, here and in Fig. S4, beyond a separation distance of approximately 200 km the coefficient of tail dependence parameter estimates drop well below 1, indicating asymptotic independence. Therefore, since separation distances within the domain extend to up to 3500 km, we conclude that asymptotic independence is the dominant extremal dependence structure across the spatial domain.

It is important to consider the validity of representing even this small proportion of asymptotically dependent pairs of locations incorrectly as asymptotically independent. To explore this, Bortot et al. (2000) carried out a simulation study in which they fit the Gaussian, Ledford and Tawn (1996), and Gumbel models to bivariate data simulated from three parent populations with different classes of extremal dependence. They concluded that, for asymptotically independent parent populations the Gaussian copula is able to provide accurate inferences for tail probability estimates, outperforming the Gumbel copula model. Indeed, even for asymptotically dependent parent populations, the estimation error of the Gaussian copula model was deemed to be acceptably small (Bortot et al., 2000). This suggests that, when data dimensionality prohibits the use of flexible extremal dependence models (e.g. Huser and Wadsworth, 2018) and asymptotic independence is found to be the dominant extremal dependence structure across the spatial domain, using an asymptotically independent model, such as the Gaussian tail model, is preferable over using a model for asymptotic dependence.

4 A conceptual loss diagnostic approach

We now contribute a natural hazard loss perspective for exploring the dominant extremal dependence class, providing further justification of the selected dependence model. We define a conceptual hazard loss function and explore the impact of misspecifying the extremal dependence class on aggregate hazard loss estimation, using the Gaussian and Gumbel copula models previously introduced. We present this approach initially based on one central location (London) and then demonstrate how this can be extended to systematically explore a high-dimensional hazard field.

Similar to other natural hazard perils, in the absence of confidential insurance industry exposure and vulnerability information, it has become common in the literature to define conceptual windstorm event loss as a function of the footprint wind gust speeds over the spatial domain (see Dawkins et al., 2016, for a review). While these conceptual windstorm loss functions vary in the detail of their composition, it is generally possible to express these loss functions as special cases of the generic loss function:

$$L(X_1, \ldots, X_m) = \sum_{j=1}^{m} e_j V\left(X_j\right) 1\left(X_j > u\left(X_j\right)\right), \tag{5}$$

where $j = 1, \ldots, m$ are the m locations in the spatial domain; V is a vulnerability function representing the damage caused by the hazard; e_j represents exposure at location j (e.g. population density); $u(X_j)$ quantifies a high threshold of the wind gust speed above which losses occur; and $1(x)$ is an indicator function such that $1(x) = 1$ if x is true

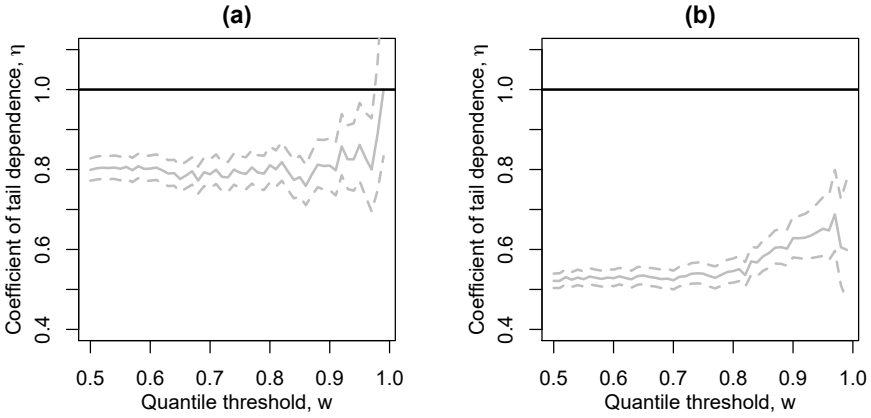

Figure 5. Diagnostic plots of maximum-likelihood estimates (solid) and 95 % profile likelihood confidence intervals (dashed) of η, in Eq. (4), for threshold w in the range of the 0.5–1 quantile of T, for London paired with **(a)** Amsterdam and **(b)** Madrid.

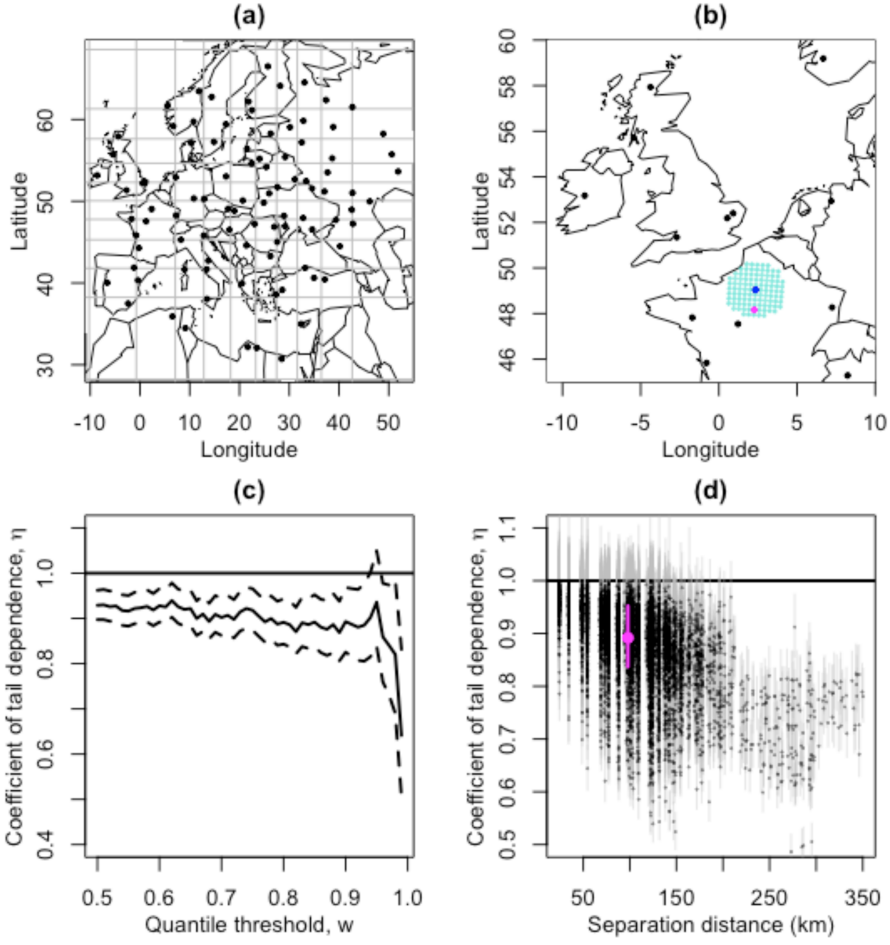

Figure 6. **(a)** A stratified (based on the distribution of locations over longitude and latitude) sample of locations within the European domain, with stratified grid shown in grey; **(b)** a demonstration of the 100 nearest locations (turquoise) to one of these sampled locations (blue), with one such point selected at random (pink); **(c)** the coefficient of tail dependence diagnostic plot (as in Fig. 5) for wind gusts at the blue location paired with the pink location; **(d)** the coefficient of tail dependence (estimated using w as the 90 % quantile threshold of the structure variable) and 95 % profile likelihood confidence intervals, for each of the 100 sampled locations paired with their 100 nearest locations in the full domain, plotted against separation distance in kilometres, with the estimate based on the pair of locations in **(b)** and **(c)** added in pink.

and $1(x) = 0$ otherwise. For example, in the widely used and rigorously validated conceptual loss function of Klawa and Ulbrich (2003), $V(X) = (X - x_{0.98})^3$, $u(X) = x_{0.98}$ (the 0.98th quantile of X), and e_j is the population density at location j, whereas Cusack (2013) used a loss function in which $V(X) = (X - x_{0.99})^3$, $u(X) = x_{0.99}$ (the 0.99th quantile of X), and $e_j = 1$ for all j. See Table 2.1 in Dawkins (2016) for a summary of previously published conceptual loss functions in terms of the components of Eq. (5).

More recently, Roberts et al. (2014) presented an exploration of the success of a number of these conceptual windstorm loss functions in representing insured loss throughout the European domain, based on the same data set as in this study, with the aim of developing a method for selecting extreme storms for the eXtreme WindStorms (XWS) catalogue. While there is much published work on the existence of a relationship between loss severity and the magnitude of the wind, in particular the cubed excess wind as used in the loss functions of Klawa and Ulbrich (2003) and Cusack (2013), Roberts et al. (2014) found that a conceptual loss function representing just the area in which the windstorm footprint exceeds a high loss threshold (i.e. $V(X_j) = 1$ and $e_j = 1$ for all j in Eq. 5) to be more successful at characterising a subset of extreme windstorms known to have caused large insured losses. It should be noted, however, that this exploration did not include population density within the Klawa and Ulbrich (2003) loss function and was therefore not a direct comparison of this measure. In addition, an alternative subjectively selected subset of extreme storms may have given an alternative result. The success of this simplistic loss function could also be due to its relative insensitivity to errors in components of the loss estimate not well represented by the climate-model-generated footprints and may not perform as well if applied to wind gust observations.

In this study we propose a similar threshold exceedance conceptual loss function to that used in Roberts et al. (2014) and Dawkins et al. (2016). Roberts et al. (2014) used an exceedance threshold of $25\,\mathrm{m\,s^{-1}}$, while Dawkins et al. (2016) used a threshold of $20\,\mathrm{m\,s^{-1}}$, as is commonly used by German insurance companies (Klawa and Ulbrich, 2003). Here, similar to Klawa and Ulbrich (2003) and Cusack (2013), we propose a locally varying wind gust speed quantile threshold, accounting for local adaptation to varying wind intensity. We find that the 0.99th quantile of windstorm footprint wind gust speed is in excess of the commonly used $20\,\mathrm{m\,s^{-1}}$ loss threshold for most land locations in Europe, with a higher loss threshold used in regions where stronger winds occur (as shown in Fig. S5).

Since, for a given storm event at any pair of locations, $e_1 V(X_1)$ and $e_2 V(X_2)$ in Eq. (5) are constants, this equation can be simplified to

$$L(X_1, X_2) \propto C_{X_1} 1(X_1 > u(X_1)) + C_{X_2} 1(X_2 > u(X_2)), \quad (6)$$

where $C_{X_1} = e_1 V(X_1)$ and $C_{X_2} = e_2 V(X_2)$. In our case $C_{X_1} = C_{X_2} = 1$, and $u(X_1) = x_{1(0.99)}$ and $u(X_2) = x_{2(0.99)}$, the 0.99th quantiles of X_1 and X_2 respectively. Therefore, while in this study we use just one conceptual loss function in which the magnitude of the loss is always equal to 1, it is simple to adapt the following analysis to accommodate alternative loss functions in which the vulnerability function is not constant across locations.

The probability mass function of the bivariate conceptual loss function can easily be obtained in terms of the extremal dependence coefficient, $\chi(p)$, by considering the joint probability of (X_1, X_2) in each of the quadrants shown in Fig. 3:

$$\begin{aligned}
&Pr\big(L(X_1, X_2) = C_{X_1} + C_{X_2}\big) = \chi(p)p,\\
&Pr\big(L(X_1, X_2) = C_{X_1}\big) = Pr\big(L(X_1, X_2) = C_{X_2}\big) = 2(1 - \chi(p))p,\\
&Pr(L(X_1, X_2) = 0) = 1 + p(\chi(p) - 2).
\end{aligned}$$

The distribution of loss is completely determined by p (which is chosen here to be 0.01) and $\chi(p)$, and so $\chi(0.01)$ can be used to diagnose and explore the consequence of extremal dependence assumptions on loss estimation. It should be noted that the expected loss, $\mathbb{E}(L(X_1, X_2))$, does not depend on $\chi(p)$. This is because the expectation of a sum is the sum of the expectations; hence expected total loss over two or more locations is simply the sum of the expected losses at each location and so is unaffected by the amount of dependency between sites.

To compare how well the Gaussian and Gumbel models represent our empirical bivariate conceptual loss function, we can therefore compare estimates for $\chi(p)$ and $\overline{\chi}(p)$ for our specified loss threshold $p = 0.01$, calculated based on each model, with those calculated empirically (as in Table A1). We present the resulting difference in these estimates for London paired with all other land locations in the European domain in Fig. 7.

Figure 7 demonstrates how well the Gaussian model is able to represent empirical $\chi(0.01)$ throughout the domain. Conversely the Gumbel model can be seen to greatly overestimate $\chi(0.01)$ for all pairs of locations. The Gaussian model also well reproduces $\overline{\chi}(0.01)$ for locations not too distant from London, with this distance being greater in the west–east direction, reflecting the common path of storms over Europe (Hoskins and Hodges, 2002). The Gumbel model greatly overestimates $\overline{\chi}(0.01)$ for all locations except those in very close proximity to London.

As well as being relevant for representing the probability mass function of the bivariate conceptual loss function, $\chi(p)$ can also be shown to characterise the conditional expectation of joint loss:

$$\begin{aligned}
\mathbb{E}(L(X_1, X_2)) &= \big(C_{X_1} + C_{X_2}\big)\chi(p)p + C_{X_1}(1 - \chi(p))p\\
&\quad + C_{X_2}(1 - \chi(p))p = \big(C_{X_1} + C_{X_2}\big)p,
\end{aligned}$$

$$\begin{aligned}
\Rightarrow &\mathbb{E}\big(L(X_1, X_2) \,|\, L(X_1) = C_{X_1}\big)\\
&= \big(C_{X_1} + C_{X_2}\big)\chi(p)p + C_{X_1}(1 - \chi(p))p\\
&= p\big(C_{X_2}\chi(p) + C_{X_1}\big). \quad (7)
\end{aligned}$$

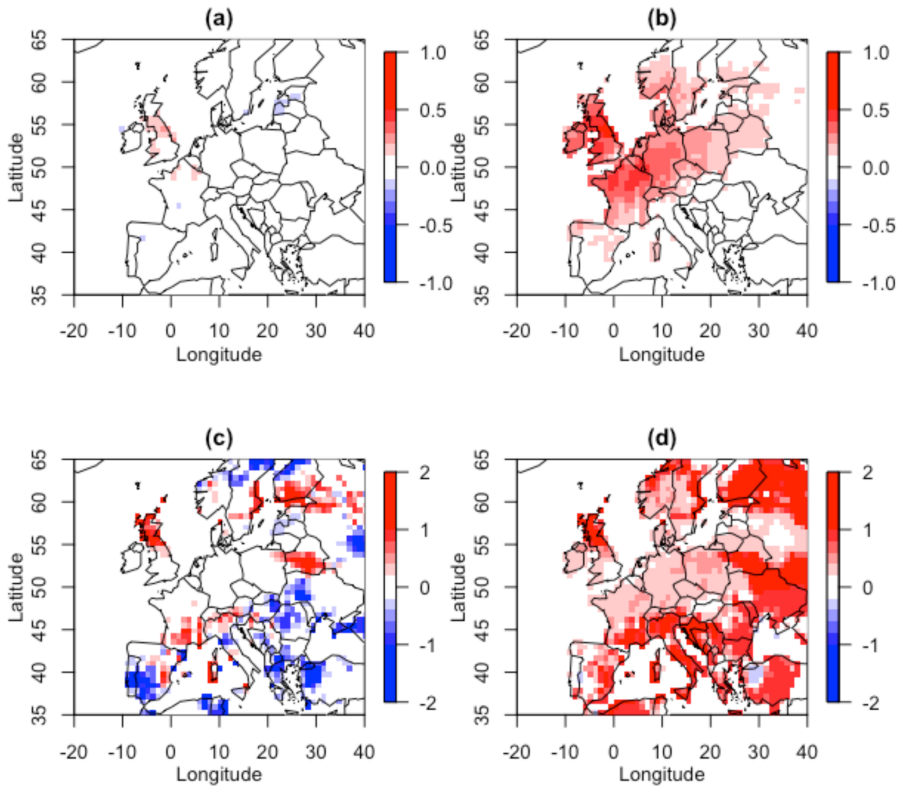

Figure 7. The difference between empirical and modelled $\chi(0.01)$ for **(a)** the Gaussian model and **(b)** the Gumbel model, and the difference between empirical and modelled $\overline{\chi}(0.01)$ for **(c)** the Gaussian model and **(d)** the Gumbel model, for London paired with all other locations over land.

The conditional first moment of the loss distribution in Eq. (7) can therefore be used to compare how well the different dependency models represent the size of the joint losses, rather than just their conditional probability of occurrence, since the expression includes C_{X_1} and C_{X_2}. Here, $C_{X_1} = C_{X_2} = 1$; hence the conditional expectation of joint loss is equivalent to the conditional expectation of loss jointly occurring at both locations given a loss has occurred at one location.

Figure 8 presents a comparison of the distribution of the conditional expected joint loss for London paired with each land location in our European domain, given a loss has occurred in London, when calculated empirically and using the two opposing dependence models.

Figure 8 further illustrates the importance of correctly specifying extremal dependence class when representing loss. When a conceptual loss occurs in London, the Gumbel dependence model overestimates the expected conditional joint loss with other European land locations, while, conversely, the Gaussian model provides a very good estimate of the empirical expected conditional joint loss distribution.

Extension to high dimensions

We extend the analysis in Fig. 7 to systematically explore the high-dimensional domain by fitting both the Gaussian and Gumbel models to a stratified sample of 100 locations paired with each of the other 99 locations and, for each pair, plot the difference between empirical and modelled $\chi(0.01)$ against their separation distance, shown in Fig. 9.

This domain-wide comparison indicates that, while the Gaussian model slightly over- and underestimates empirical $\chi(0.01)$ at small separation distances, this model consistently outperforms the Gumbel model, which overestimates $\chi(0.01)$ for all separation distances, even very small ones. This indicates, as in Fig. 6, that a majority of nearby locations do not exhibit asymptotic dependence as they are not well represented by the Gumbel model, further supporting the diagnosed dominance of extremal independence throughout the European domain.

Finally, we extend the analysis in Fig. 8 to systematically explore the high-dimensional domain by replacing London as the location of origin, with each location within a stratified sample of 100 locations. For each of these 100 locations, Fig. 10 presents the difference between modelled and empirical relative frequencies of binned ranges of conditional

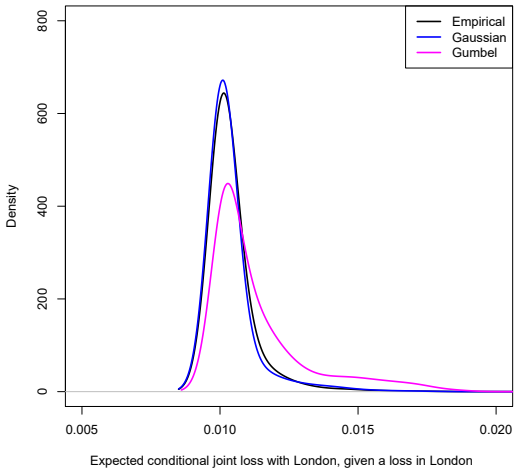

Figure 8. For all land locations in the European domain, the conditional expected joint loss with London, given a loss has occurred in London (Eq. 7), calculated empirically and using the Gaussian and Gumbel copula models.

expected joint loss, separately for the Gaussian and Gumbel models, i.e. representing the difference between the modelled and empirical density plots in Fig. 8, but for 100 locations rather than one. Figure 10b identifies that the discrepancy between the empirical and Gumbel estimates of conditional expected joint loss shown in Fig. 8 is consistent throughout the domain, with lower values being under-represented and higher values over-represented by the Gumbel model. In a similar way, Fig. 10a shows that the Gaussian model performs equally well for these 100 locations, with much smaller discrepancy compared to the Gumbel model, as found in Fig. 8.

In this windstorm footprint application, we found that, while the Gumbel model is able to represent some pairs of locations at very small separation distances, where asymptotic dependence is suggested by the coefficient of tail dependence, this model greatly misrepresents the joint-tail behaviour and hence the conditional probability of joint loss for a majority of pairs and separation distances. Conversely, the Gaussian model is able to represent the joint-tail behaviour relevant for loss estimation for locations within close proximity to each other, as well as further apart.

As previously mentioned, alternative windstorm loss thresholds have been implemented in other studies, for example the 0.98th quantile in Klawa and Ulbrich (2003), and the fixed thresholds of $20\,\mathrm{ms}^{-1}$ in Bonazzi et al. (2012) and Dawkins et al. (2016) and $25\,\mathrm{m\,s}^{-1}$ in Lamb and Frydendahl (1991) and Roberts et al. (2014). An exploration of the effect of the choice of loss threshold and, indeed loss function, on how the opposing dependence models represent joint losses would be an extremely interesting area of further investigation but is beyond the scope of this study. Dawkins (2016) goes some way in addressing this by presenting a comparison for the 0.98th quantile and $25\,\mathrm{m\,s}^{-1}$ fixed loss thresholds in the same form as Fig. 7. Dawkins (2016) found that the overall suitability of the opposing models remained the same for both thresholds, although the discrepancy of the Gumbel model was slightly smaller for the lower, 0.98th quantile loss threshold. This was thought to be because modelled exceedances further from the upper limit of the joint distribution were less sensitive to a misspecification of the extremal dependence characteristic in the Gumbel model.

5 Why are wind gust speeds asymptotically independent?

It is of interest to ask whether there might be fundamental fluid dynamical reasons for why extreme wind gust speeds should be asymptotically independent at different spatial locations. One approach to answering this question is to consider extremal dependence in turbulent flows. The atmospheric flow in storm track regions is highly chaotic and irregular and is therefore turbulent rather than smoothly varying laminar flow (see Held, 1999, and references therein). Furthermore, over short enough spatial distances, the horizontal flow in a storm may be considered to be stationary in space and directionally invariant, in other words, homogeneous isotropic turbulence.

It is useful to first consider the more tractable problem of dependency in simultaneous wind speeds rather than maximum wind speeds over a given time period. The dependency between maximum gust speeds over 3 days will not generally be less than the dependency between simultaneous wind gust speeds because maximum wind gusts for a storm do not occur at the same time at different locations. However, for locations that are close to one another, maximum gust speeds for fast-moving extreme storms will occur within a short time window (e.g. within around 3 h or less for extreme storms over the UK), and so simultaneous results become more relevant.

As originally proposed by Von Kármán (1937), turbulent wind fields can be efficiently and realistically simulated using stochastic processes (Mann, 1998). This approach is widely used for many applications such as testing loads on new aircraft designs. The basic assumption in homogeneous turbulence is that the Cartesian velocity components are independent Gaussian processes, each with a prescribed spatial covariance function. In the special case of isotropic turbulence, the spatial covariance functions are identical for each velocity component. Hence, for two-dimensional windstorm gusts, the wind gust speed at spatial location j is given by $X_j = \sqrt{u_j^2 + v_j^2}$, where u_j and v_j are independent Gaussian processes having identical covariance functions.

The distribution of each velocity component is expected, by the central limit theorem, to be close to normally distributed since the net displacement of a particle in turbulence is the result of many irregular smaller displacements. The

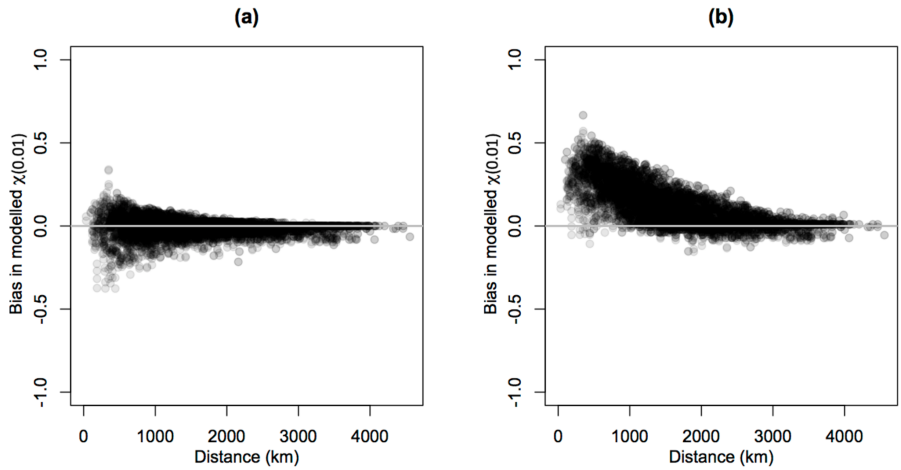

Figure 9. The difference between empirical and modelled $\chi(0.01)$ for a stratified sample of 100 locations paired with each of the other 99 locations, plotted against separation distance for **(a)** the Gaussian model and **(b)** the Gumbel model.

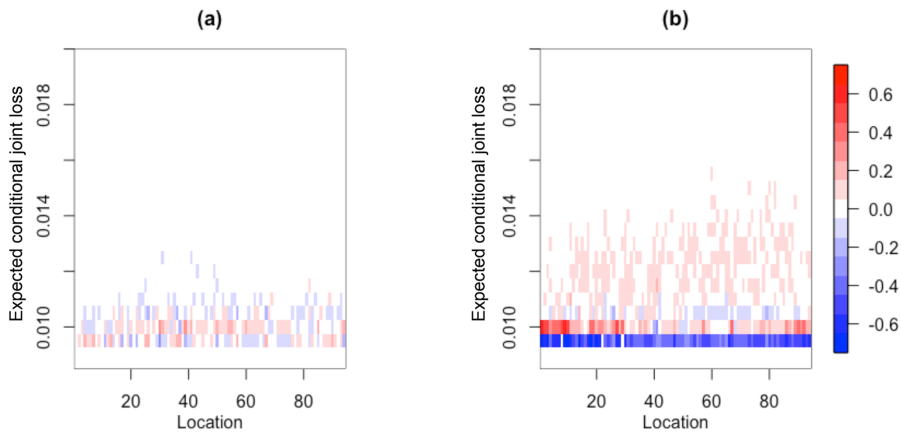

Figure 10. For a stratified sample of 100 locations within the windstorm footprint domain, the difference between modelled and empirical relative frequencies of binned ranges of expected conditional joint loss for **(a)** the Gaussian model and **(b)** the Gumbel model.

distribution of each component has zero skewness due to the symmetry of the fluid equations (negative deviations are as likely as positive ones) but can have slightly more kurtosis (i.e. fatter tails) than the normal distribution due to intermittency in the flow. Measurements of velocity components in the atmospheric surface layer reveal that the distributions are near to Gaussian (e.g. Chu et al., 1996).

So what can be deduced about the extremal dependence class of wind speeds from such turbulence models? Firstly, as shown in example 5.32 of McNeil et al. (2005), since the individual velocity components are bivariate normal, the individual velocity components are asymptotically independent at different locations; e.g. u_1 and u_2 are asymptotically independent when locations $j = 1$ and $j = 2$ differ, and likewise for v_1 and v_2. Furthermore, it can be shown that the square of each velocity component is also asymptotically independent (see Appendix).

The squared wind speeds at pairs of locations are sums of two such independent components, $(X_1^2, X_2^2) = (u_1^2 + v_1^2, u_2^2 + v_2^2)$, and so it would be counter-intuitive if somehow these sums were not also asymptotically independent. Unfortunately proof of asymptotic independence between (X_1^2, X_2^2) (and hence (X_1, X_2)) remains elusive. Nevertheless, the conjecture can be explored using numerical simulation.

By simulating velocities from bivariate normal distributions, we have found no evidence of extremal dependence in wind speeds even when each velocity component is highly correlated. Figure 11 shows an example obtained by simulating a million wind speeds at two locations where the u and v velocity components are independent standard normal variates each with correlation of 0.9 between locations (i.e. the correlation between u_1 and u_2 is 0.9). The squared wind speeds at each location are chi-squared distributed with 2° of freedom but are not independent: there is positive association clearly visible in Fig. 11a. To assess extremal depen-

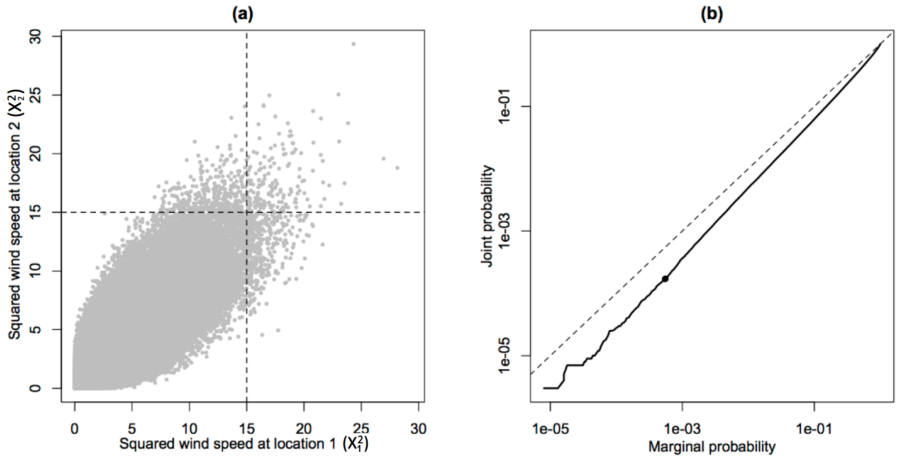

Figure 11. Simulation of wind speeds at two sites having highly correlated velocities (see main text for details): **(a)** scatter plot of squared wind speeds at the two sites (1000 points randomly sampled out of the million); **(b)** joint versus marginal exceedance probabilities (on logarithmic axes). The dot shows an example obtained by counting the fraction of points in the upper right and the right-hand quadrants of **(a)**. The curve has a steeper slope than the dashed line (equal probabilities denoting complete dependence), suggesting asymptotic independence.

dence, Fig. 11b shows how the joint exceedance probability, $Pr(X_1^2 > t^2,\ X_2^2 > t^2)$, and the marginal exceedance probability, $Pr(X_1^2 > t^2) = Pr(X_2^2 > t^2)$, behave as threshold t^2 is varied. As the threshold is increased, the joint probability drops to zero faster than the marginal exceedance probability (the curve in Fig. 11b is steeper than the dashed line), which suggests that the ratio, the conditional probability of exceedance, equivalent to χ in Eq. (1), will tend to zero in the asymptotic limit.

6 Conclusion

This study has demonstrated how to use the extremal dependence diagnostics of Coles et al. (1999) and Ledford and Tawn (1996) along with the Gaussian and Gumbel copula models to explore and identify the dominant extremal dependence class in a very high dimensional natural hazard field. Furthermore, we have explicitly shown how extremal dependency determines conceptual aggregate loss functions and have revealed how sensitive the aggregate loss distribution is to misspecification of extremal dependency.

These methods present strong evidence for asymptotic independence in windstorm footprint hazard fields, contrary to what has been assumed in previous studies such as Bonazzi et al. (2012). The misspecification of this extremal dependency (e.g. by using a Gumbel copula) has been shown to lead to severe overestimation of the aggregate losses. Stochastic turbulence theory suggests that asymptotic independence of wind speeds is a generic property of turbulent flows as seen in windstorm footprints. These results provide justification that simulated windstorm hazard fields can be represented by a Gaussian geostatistical model (Dawkins, 2016; Youngman and Stephenson, 2016).

Data availability. The windstorm footprint data set used in this paper is not available, but 50 of the 6103 storms can be accessed in the XWS catalogue at http://www.europeanwindstorms.org/ (European Wind Storms, 2018).

Appendix A

Table A1. Empirical and parametric forms for extremal dependence measures $\chi(p)$ and $\overline{\chi}(p)$.

	$\chi(p)$	$\overline{\chi}(p)$
Empirical	$\frac{a}{a+c}$	$\frac{2\log(a+c)/n}{\log(a/n)} - 1$
Power law	$\frac{1}{n}\exp\left(\frac{\alpha}{\eta}\right)p^{\frac{1}{\eta}-1}$	$\frac{2\log(p)}{\log\left(\frac{1}{n}\exp\left(\frac{\alpha}{\eta}\right)\right)+\frac{1}{\eta}\log(p)} - 1$
Gumbel	$\sim 2 - \frac{(2\log(1-p)^r)^{\frac{1}{r}}}{\log(1-p)} = 2 - 2^{\frac{1}{r}}$ (Coles et al., 1999)	$\frac{2\log(p)}{\log(2p(1-p)^2)} - 1$
Gaussian	$\overline{F}(1-p, 1-p)/p$, where $\overline{F}(1-p, 1-p) = Pr\left(X_1 > x_{1(1-p)}, X_2 > x_{2(1-p)}\right) \sim (1+\rho)^{\frac{3}{2}}(1-\rho)^{\frac{1}{2}}(4\pi)^{-\frac{\rho}{1+\rho}} (-\log(p))^{\frac{\rho}{1+\rho}} p^{\frac{2}{1+\rho}}$ as $p \to 0$(Coles et al., 1999)	$\frac{2\log(p)}{\log(\overline{F}(1-p,1-p))} - 1$

Appendix B: Proof of independence in stochastic models of turbulent flows

Assume the velocity components (u_1, v_1) and (u_2, v_2) at two separate locations in an isotropic turbulent flow can be represented as bivariate normally distributed vectors (u_1, u_2) and (v_1, v_2) that are independent and identically distributed with zero expectations.

The individual velocity components, (u_1, u_2) and (v_1, v_2), are both asymptotically independent because of each being bivariate normally distributed.

The squares of the individual velocity components, e.g. (u_1^2, u_2^2), are also asymptotically independent. This is proven by rewriting the joint probability of exceedance:

$$\begin{aligned}
&Pr\left(u_1^2 > t^2, u_2^2 > t^2\right) \\
&\quad = Pr(u_1 > t, u_2 > t) + Pr(u_1 > t, u_2 \le t) \\
&\quad + Pr(u_1 \le t, u_2 > t) + Pr(u_1 \le t, u_2 \le t) \\
&\quad = \chi_{++}Pr(u_1 > t) + \chi_{-+}Pr(u_1 > t) \\
&\quad + \chi_{-+}Pr(u_1 \le t) + \chi_{--}Pr(u_1 \le t) \\
&\quad = \chi_{++}Pr\left(u_1^2 > t^2\right) + \chi_{+-}Pr\left(u_1^2 > t^2\right),
\end{aligned}$$

which is obtained by noting that $Pr(u_1^2 > t^2) = Pr(u_1 > t) + Pr(u_1 \le t)$, and conditional probabilities $\chi_{++} = \chi_{--}$ and $\chi_{+-} = \chi_{-+}$ by symmetry of the bivariate normal distribution about (0, 0). Since the components are bivariate normal, χ_{++} and $\chi_{+-} \to 0$ as $t \to \infty$, and so $Pr(u_1 2 > t^2, u_2^2 > t^2)/Pr(u_1^2 > t^2) \to 0$. Hence, the square of the velocity component is also asymptotically independent.

Perhaps rather counter-intuitively, the sum of two independent identically distributed asymptotically independent variables is not necessarily asymptotically independent. It, therefore, remains to be proven whether or not $(u_1^2 + v_1^2, u_2^2 + v_2^2)$ is asymptotically independent.

Supplement. The supplement related to this article is available online at: https://doi.org/10.5194/nhess-18-2933-2018-supplement.

Author contributions. Sections 1–4 of this study were developed and written by LD, based on chap. 3 of her PhD thesis, supervised by DS. Section 5 was conceived and written by DS.

Competing interests. The authors declare that they have no conflict of interest.

Acknowledgements. Laura C. Dawkins was supported by the Natural Environment Research Council (Consortium on Risk in the Environment: Diagnostics, Integration, Benchmarking, Learning and Elicitation – CREDIBLE project; NE/J017043/1).

Edited by: Joaquim G. Pinto
Reviewed by: three anonymous referees

References

Blanchet, J., Marty, C., and Lehning, M.: Extreme value statistics of snowfall in the Swiss Alpine region, Water Resour. Res., 45, W05424, https://doi.org/10.1029/2009WR007916, 2009.

Bonazzi, A., Cusack, S., Mitas, C., and Jewson, S.: The spatial structure of European wind storms as characterized by bivariate extreme-value Copulas, Nat. Hazards Earth Syst. Sci., 12, 1769–1782, https://doi.org/10.5194/nhess-12-1769-2012, 2012.

Bortot, P., Coles, S., and Tawn, J.: The multivariate Gaussian tail model: an application to oceanographic data, Appl. Stat., 49, 31–49, 2000.

Chu, C. R., Parlange, M. B., Katul, G. G., and Albertson, J. D.: Probability density functions of turbulent velocity and temperature in the atmospheric surface layer, Water Resour. Res., 32, 1681–1688, 1996.

Coles, S. G.: An Introduction to Statistical Modeling of Extreme Values, Springer, London, 2001.

Coles, S. G. and Walshaw, D.: Directional Modelling of Extreme Wind Speeds, J. Roy. Stat. Soc. C, 43, 139–157, 1994.

Coles, S. G., Heffernan, J., and Tawn, J.: Dependence Measures for Extreme Value Analysis, Extremes, 2, 339–365, 1999.

Cusack, S.: A 101 year record of windstorms in the Netherlands, Climatic Change, 116, 693–704, 2013.

Dawkins, L. C.: Statistical modelling of European windstorm footprints to explore hazard characteristics and insured loss, PhD thesis, University of Exeter, College of Engineering Mathematics and Physical Sciences, Exeter, 2016.

Dawkins, L. C., Stephenson, D. B., Lockwood, J. F., and Maisey, P. E.: The 21st century decline in damaging European windstorms, Nat. Hazards Earth Syst. Sci., 16, 1999–2007, https://doi.org/10.5194/nhess-16-1999-2016, 2016.

de Fondeville, R. and Davison, A. C.: High-dimensional peaks-over-threshold inference, Biometrika, 0, 1–18, 2018.

Dee, D., Uppala, S. M., Simmons, A. J., Berrisford, P., Poli, P., Kobayashi, S., Andrae, U., Balmaseda, M. A., Balsamo, G., Bauer, P., Bechtold, P., Beljaars, A. C. M., van de Berg, L., Bidlot, J., Bormann, N., Delsol, C., Dragani, R., Fuentes, M., Geer, A. J., Haimberger, L., Healy, S. B., Hersbach, H., Hólm, E. V., Isaksen, L., Kallberg, P., Kohler, M., Matricardi, M., McNally, A. P., Monge-Sanz, B. N., Morcrette, J. J., Park, B. K., Peubey, C., de Rosnay, P., Tavolato, C., Thepaut, J. N., and Vitart, F.: The ERA Interim reanalysis: configuration and performance of the data assimilation system, Q. J. Roy. Meteorol. Soc., 137, 553–597, 2011.

Eastoe, E. F., Koukoulas, S., and Jonathan, P.: Statistical measures of extremal dependence illustrated using measured sea surface elevations from a neighbourhood of coastal locations, Ocean Eng., 62, 68–77, 2013.

European Wind Storms: Extreme Wind Storms (XWS) Catalogue, available at: http://www.europeanwindstorms.org/, last access: 7 November 2018.

Ferro, C. A. T.: A Probability Model for Veryfiying Deterministic Forecasts of Extreme Events, Weather Forecast., 22, 1089–1100, 2007.

Haylock, M. R.: European extra-tropical storm damage risk from a multi-model ensemble of dynamically-downscaled global climate models, Nat. Hazards Earth Syst. Sci., 11, 2847–2857, https://doi.org/10.5194/nhess-11-2847-2011, 2011.

Heffernan, J. E. and Tawn, J. A.: A conditional approach for multivariate extreme values, J. Roy. Stat. Soc. B, 66, 497–546, 2004.

Held, I. M.: The macroturbulence of the troposphere, Tellus A, 51, 59–70, 1999.

Hodges, K. I.: Feature Tracking on the Unit Sphere, Mon. Weather Rev., 123, 3458–3465, 1995.

Hoskins, B. J. and Hodges, K. I.: New Perspectives on the Northern Hemisphere Winter Storm Tracks, J. Atmos. Sci., 59, 1041–1061, 2002.

Huser, R. G. and Davison, A. C.: Space–time modelling of extreme events, J. Roy. Stat. Soc. B, 76, 439–461, 2013.

Huser, R. G. and Wadsworth, J. L.: Modeling spatial processes with unknown extremal dependence class, J. Am. Stat. Assoc., in press, 2018.

Huser, R. G., Opitz, T., and Thibaud, E.: Bridging asymptotic independence and dependence in spatial extremes using Gaussian scale mixtures, Spatial Stat., 21, 166–186, 2017.

Kereszturi, M., Tawn, J., and Jonathan, P.: Assessing extremal dependence of North Sea storm severity, Ocean Eng., 118, 242–259, 2015.

Klawa, M. and Ulbrich, U.: A model for the estimation of storm losses and the identification of severe winter storms in Germany, Nat. Hazards Earth Syst. Sci., 3, 725–732, https://doi.org/10.5194/nhess-3-725-2003, 2003.

Lamb, H. and Frydendahl, J.: Historic Storms of the North Sea, British Isles and Northwest Europe, Cambridge University Press, Cambridge, 1991.

Ledford, A. W. and Tawn, J. A.: Statistics for near independence in multivariate e xtreme values, Biometrika, 83, 169–187, 1996.

Ledford, A. W. and Tawn, J. A.: Modelling Dependence within Joint Tail Regions, J. Roy. Stat. Soc., 59, 475–499, 1997.

Mann, J.: Wind field simulation, Probabil. Eng. Mech., 13, 269–282, 1998.

McNeil, A. J., Frey, R., and Embrechts, P.: Quantitative Risk Management: Concepts, Techniques, Tools, Princeton University Press, Princeton, 2005.

Nelson, R. B.: An Introduction to Copulas, 2nd Edn., Springer, New York, 2006.

Panofsky, H. A., Tennekes, H., Lenschow, D. H., and Wyngaard, J. C.: The characteristics of turbulent velocity components in the surface layer under convective conditions, Bound.-Lay. Meteorol., 11, 355–361, 1977.

Roberts, J. F., Champion, A. J., Dawkins, L. C., Hodges, K. I., Shaffrey, L. C., Stephenson, D. B., Stringer, M. A., Thornton, H. E., and Youngman, B. D.: The XWS open access catalogue of extreme European windstorms from 1979 to 2012, Nat. Hazards Earth Syst. Sci., 14, 2487–2501, https://doi.org/10.5194/nhess-14-2487-2014, 2014.

Sheridan, P.: Review of techniques and research for gust forecasting and parameterisation: Forecasting Research Technical Report 570, Tech. rep., Met Office, Exeter, UK, 2011.

Von Kármán, T.: The fundamentals of the statistical theory of turbulence, J. Aeronaut. Sci., 4, 131–138, 1937.

Wadsworth, J. L. and Tawn, J. A.: Dependence modelling for spatial extremes, Biometrika, 99, 253–272, 2012.

Wadsworth, J. L., Tawn, J. A., Davison, A. C., and Elton, D. M.: Modelling across extremal dependence classes, J. Roy. Stat. Soc. B, 79, 149–175, 2017.

Youngman, B. D. and Stephenson, D. B.: A geostatistical extreme-value framework for fast simulation of natural hazard events, Proc. Math. Phys. Eng. Sci., 472, 20150855, https://doi.org/10.1098/rspa.2015.0855, 2016.

EXECUTIVE SUMMARY

In an anthropocentric world increasingly defined by changes in atmospheric chemistry, two clear trends have emerged. One is the increase in the frequency and severity of extreme and anomalous weather events, the latter driven by rising temperatures and changing patterns of humidity and precipitation; the other is the rapid acceleration of photovoltaic (PV) capacity, including the spread of PV into new climate zones, with 2 terawatts (TW) deployed across six continents in 2024, and on course for an expected 8 TW by 2030.

To ensure the further growth of PV energy generation worldwide requires attention be paid to global climate trends and to opportunities for designing PV systems to withstand and quickly recover from specific storm threats. Traditionally, solar technologies have been a one-size-fits-all commodity, and specific climatic stressors have been a minor consideration in module and system design. As solar installations proliferate across almost all climate zones, however, design optimization for specific weather threats is gaining attention. This report provides a comprehensive look at changing weather patterns and their anticipated impact on the reliability and performance of PV systems worldwide. Broken down by storm category, the report covers extreme weather events of greatest significance to PV power plants: tropical cyclones, convective storms, snowstorms, dust storms, heat waves, floods and wildfires. For each category, an overview of the threat landscape is provided, along with best practices for design and procurement, mitigation strategies, post-storm assessment and follow-on operation and maintenance (O&M) strategies.

The report also considers weather-inflicted damages to PV systems that fall into one of two categories:

1) catastrophic, as in, the destruction of modules, strings or entire systems, e.g., modules unravel from their mounts, racks collapse, and glass shatters; and 2) sub-catastrophic, as in, visual inspection results in no detectable damage, even though internal damage may have occurred to the solar cells or other module components, Detectable only with costly imaging techniques, such as infrared (IR) or electroluminescence (EL) imaging, undiagnosed damage may deteriorate over time, resulting in accelerated performance degradation or the accelerated senescence of module components, such as backsheets and encapsulants.

In addition, the report acknowledges that technological innovation in the solar industry, including the proliferation of new materials and components, introduces uncertainty in a world of intensifying climatic stressors. The long-term reliability of emerging cell and module architectures is largely unknown, especially under extreme-weather conditions where modules and hardware components are subjected to combined and cyclic forces not captured by accelerated testing.

Moreover, the resilience of a PV system during extreme weather depends heavily on the unique characteristics of each storm — including the number and types of stressors, how these stressors interact in predictable and unpredictable ways, and how such interactions affect the system's components. Even so, generalizations around best practices can be made: 1) site planning should always include a review of weather threats specific to the site; and 2) design and procurement decisions should be based on the threat landscape. In hail-prone regions, for example, modules with thicker front glass are preferred; in snowy regions, frameless outperform framed modules; in regions where tropical cyclones are the primary risk, consideration must be paid not only to the module architecture but even more to the fasteners and other hardware that hold the system together. Stow algorithms for single-axis trackers should also be validated via tracked records of damage prevention. In addition, each site must have a set of protocols and response strategies specific to the weather threat and be prepared to follow them on short notice. And last, but not least, the operational status of a plant must be

considered. Sites under construction are more prone to erosion because ground cover is lacking, to wind damages because modules may not be properly fastened and are susceptible to flying debris, and to electrical damages, if cable and connectors are exposed to moisture. In contrast, fully operational plants are at risk of onsite fires from damages to the electrical network and may have prolonged power losses.

Key Takeaways

1. Most PV plants can survive most extreme weather events, if appropriately sited, designed and maintained.

2. This report considers weather events that 1) have short-term impacts and occur sporadically, e.g., tropical cyclones, convective storms (including hail) and 2) those that have longer-term impacts and tend to be repetitive, e.g., snow, dust storms, heatwaves, and wildfires. From an impact perspective, two types of damage can be identified in PV systems: acute and chronic. Risk assessment for PV plants in the first category is a critical first step, whereas design optimization for plants in the second is the priority. From a resilience and mitigation standpoint, site planning is essential. Risk assessment based on a review of historical weather data and the probability of future extreme weather events for each location is crucial and must be addressed in the design phase. Once the threat landscape has been properly assessed, project developers, and owners must make informed design and procurement choices. All materials and structural components must be code-compliant; module architecture also matters, as in, modules specifically designed for hail resilience. In addition, review of the racking/tracking design, including hardware, by an independent engineer is strongly encouraged. In addition, architects should pay close attention to the terrain and geological conditions at the proposed site. For example, when installing a PV system on sloped ground, the foundation should include features to prevent landslides triggered by tropical cyclones or flooding.
3. Site owners and operators should keep relevant commissioning documents, particularly those related to energy production in order to have a baseline against which future performance can be compared. Similarly, any electroluminescent (EL) and infrared (IR) images, along with records of visual inspections and I-V measurements, should be preserved.
4. Electrical performance data are essential for evaluating the effects of extreme weather events and any resulting acceleration in system degradation. When combined with weather data—such as temperature, solar irradiation, and wind speed—this information forms time-series data that can help detect weather-related damage. Awareness among site owners and maintenance teams needs to increase regarding the importance of collecting and preserving these data.
5. Robust operation and maintenance (O&M) protocols are essential. Defects left unresolved after storm exposure may worsen over time when exposed to additional environmental stressors like heat, wind, and moisture. Continuous monitoring of power output from restored PV systems is therefore critical to ensure their performance and reliability. If a significant drop in power generation is detected, the collected data will help the owner make informed decisions about further actions, such as system refurbishment.
6. Proactive maintenance is equally important and should be tailored to the probability of risk. Before a tropical cyclone, for example, tasks such as checking the t tightness of

PV systems installed in coastal areas in North America and Asia are considered most at risk from tropical cyclones [1], [5], as seen in Figure 5. Furthermore, as storm activity expands, regions previously unaffected by intense storms may be at risk, exemplified by Hurricane Helene, which in 2024 devasted an area of North Carolina more than 500 miles (≃ 805 km) inland.

2.2 Equipment damage and failure mechanisms

Storm damages are generally attributable to poorly designed racking systems and/or poorly installed bolts and fasteners. Fasteners that are inadequately torqued or not designed for high-stress conditions (as in having low mechanical strength) are a common problem. Fretting and the resultant wear of threaded bolts can lead to loosening during wind events—and if the wind load is severe enough—cause cascading effects that range from the collapse of the racking or tracker platform to modules being ripped from their fasteners, often in multiples (see Figure 6). In addition, excessive, repetitive wind loads can lead to irreversible deformation of both fasteners and support structures if they exceed the allowable stress of the mounting hardware.

Figure 6: Tracker system damaged by Hurricane Helene in the US in 2024 is shown here. Fastener failures caused modules to detach from the torque tube and tear from electrical connections.

Tracking systems, where modules are attached to a single torque tube fixed on one end, are vulnerable to torsional stress that is exacerbated by high wind loading on the modules. If the hardware is insufficient for the wind load, strong winds can induce torsional galloping, creating escalating stress on the modules, resulting in a runaway-failure event. The process begins when the end-of-row modules begin to flutter and then twist inward from the edges toward the central modules, which are supported by the drive mechanism and are therefore the most rigid part of the row. As the outer modules loosen, the twisting gradually intensifies, spreading from one module to another. Eventually, the tracker will twist apart, resulting in airborne modules and the loss of the entire row [9].

Damage may also extend beyond mechanical failures to include a heightened risk of electrical failure. High winds can loosen cables, causing fretting within connectors and/or partial separation of the pin and socket. Loose or poorly torqued connectors then become vulnerable to moisture penetration, which in turn leads to corrosion, high resistance and ultimately failure [10]. Heavy rainfall can also lead to water penetration inside the housing of combiner boxes/power conditioner boxes, disrupting the electrical circuitry throughout a plant.

2.3 Economic impacts

The economic impacts of tropical cyclones on PV plants are manifold, ranging from lost generation to physical damages to increased operating expenses. One study of generation losses during 18 hurricane events, showed power losses of approximately 50% during the period of storm activity (likely attributable to a combination of trackers in stow position and reduced irradiance), although generation returned to normal afterwards [11]. Statistical analysis also revealed that the performance ratio during hurricane days was—as might be expected—12.6%

lower than on non-hurricane days [12]. Recent data, however, suggests that annual production losses (median values) due to high winds and heavy rain are relatively small, around 1% for each category [13]. The same study suggests that degradation rates for PV systems accelerate for sites which exceed a minimum wind speed threshold (25 m/s = 90 km/h) [13]. As explained by the authors, this effect may vary depending on the surrounding environment (e.g., wind shadowing) and/or appropriate operation and maintenance practices. While more data is needed, it appears feasible to predict generation losses due to tropical cyclones and incorporate those predictive models into the design and procurement stages for new plants to ensure more accurate LCOE calculations and provide a justification for more robust designs.

Such probability modelling is increasingly justifiable based on the escalating frequency and rising costs of storm events. As the number of PV installations grows, insurance payouts for severe-weather damage are likely to rise. In Japan, for example, insurance payouts increased by a factor of 3.7 from 2017 to 2021 [14], with a significant portion attributed to damages from high winds, flooding, and related causes [15]. Much as the intensity of tropical cyclones is expected to increase [1], insurance rates for PV systems are also likely to rise, commensurate with the heightened risk of severe damage. This represents an indirect, but measurable, economic impact of extreme weather.

2.4 Diagnostic tools

Two types of post-storm assessments are needed to a diagnose the damage caused by tropical cyclones: 1) an electrical analysis to accurately estimate the storm's impacts on electrical safety and power production; and 2) a structural analysis to document any physical damages to modules, racking and associated hardware. Daily or real-time monitoring of PV electrical systems in areas prone to tropical cyclones is highly advisable and various service providers offer monitoring systems with advanced technologies (e.g., their own PV performance software). If a properly monitored PV system shows an abnormal reduction in electrical generation during or after a tropical cyclone, electrical safety must be promptly confirmed. In particular, combiner boxes, inverters and high-voltage equipment enclosures should be checked for ingress of wind-driven rain. Drone-mounted or handheld thermal cameras can also be deployed to verify the electrical safety of PV connectors. Less urgent from a safety perspective is the diagnosis of damage to the solar cells in the absence of broken module glass. The latter involves subjecting a subset of modules to EL-imaging but the process is time-consuming and expensive and generally undertaken only if there is reason to suspect cell damage, and—even then—may involve only a sampling of modules (for more information on EL imaging, see Chapter 3).

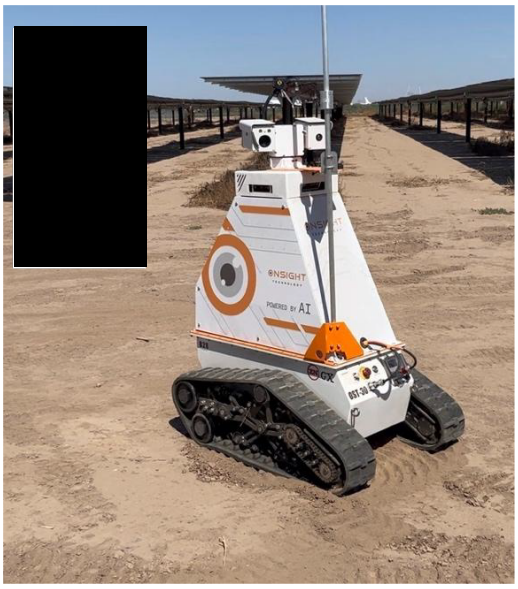

Figure 7: Ground-level robots, equipped with thermal and optical cameras can image front and rear-sides of the modules, as well as the rear-side electrical network. Photo: [redacted]

In addition to employing aerial drones to survey the site and document site-wide damages (e.g., number and location of damaged modules/rows), manual inspections are needed to

ascertain structural damage. Although Light Detection and Ranging (LiDAR) technology (with or without an unmanned aerial vehicle) could be valuable in the future [16], best practices today call for a detailed row-by-row inspection to assess the integrity of the modules, racking hardware and electrical BoS. Ground-level robots that survey each module and take thermal images of the connectors, are a technology that is gaining interest, especially for the largest PV plants, (see Figure 7) but have yet to become commonplace. New-generation drones that can fly between the rows and also capture backside images are also attracting interest but require more sophisticated controls and navigation software.

2.5 Mitigation strategies

Because PV installations are proliferating in tropical and sub-tropical regions, damages to PV systems from tropical cyclones are on the rise. To mitigate the escalating threat posed by severe winds and heavy rain, best practices (summarized in Table 1) can be categorized into four stages as follows: 1) project planning, 2) system design, 3) construction and commissioning, 4) operation and maintenance.

In the *project planning stage*, it is important to consider the historic patterns of tropical cyclone activity (see Table 2). This information is crucial for determining whether a specific location is high or low risk for a catastrophic storm and whether or not a resilient PV system can be designed for that site. For example, one can estimate both the capital expenditure (CAPEX) and operational expenditure (OPEX) for a proposed PV system based on the relevant meteorological parameters, e.g., wind speed, precipitation, etc. Analysis of historical wind patterns is also advised because predominant wind direction as well as its ramp rate can inform tracker stow strategies.

The *design phase*, however, is the crucial stage for mitigating serious damage [17]. Detailed design recommendations for PV systems installed in cyclone-prone areas are shown in Table 3. System designers should adhere to these guidelines to ensure that materials for structural components and PV modules are chosen within the specified limits set by these regulations. In addition, the recommendations described in the chapter 5.6.5 of “Guidelines for Operation and Maintenance of Photovoltaic Power Plants in Different Climates” should be considered [10]. The authors of this report also strongly recommend that the choice of a racking/tracking system be reviewed by an independent engineer, with expertise in bolted joints and failure mechanisms specific to climatic stressors.

During *construction and commissioning,* installation training is paramount, and field crews should be explicitly trained to properly install module fasteners as well as bolted joints, which are widely acknowledged to be the weak point in many racking systems and insufficiently covered by existing codes and standards. For example, current PV auditing standards, such as IEC 62446, do not include checks for fasteners or torque audits despite their importance to system reliability. At the commissioning stage, the agent of record should (1) verify the correct installation of all—or a significant subset of—designated structural connections, and (2) conduct torque audits on at least 1% of the fasteners. If 10% or more of these fasteners are either over-tightened or under-tightened, the contractor should reinstall all fasteners [18]. In addition, the improper management of electrical cables poses significant risks to the integrity of the PV connectors and ultimately the electrical balance-of-systems. Other poor practices that should be avoided include loose hanging wires, widespread reliance on plastic cable ties, and improper routing of PV wires [19].

During the *O&M* stage, the site-owner or site-operator should implement clear protocols for pre- and post-storm O&M tasks, including stow strategies for tracking systems in advance of a storm and post-storm inspections that include module examinations, torque tests of fasteners

and thermal imaging of connectors [20]. While these tasks can be performed by onsite personnel, hiring skilled consulting engineers to manage the recovery efforts is recommended. In addition, safety checks conducted by a qualified electrician are essential before accessing the system [20].

2.6 Key takeaways and recommendations

In regions prone to frequent cyclones, project planning should include an overall risk assessment, accounting for historical and predicted weather patterns as well as design and procurement decisions. In plain words, historical weather conditions, as well as future projections, should inform the planning stage and be reflected in each specific site design.

Pre- and post-storm planning for existing, as well as partially constructed, PV systems, is also of high importance. Such planning includes both installation and response training for onsite crews and the dissemination of detailed protocols to minimize confusion and maximize both response and recovery strategies. A rapidly executed pre-storm response — in accordance with the weather forecast and alarms reported by various agents (Table 2) — should be integral to any onsite operations manual. The following countermeasures are minimum requirements.

Pre-storm phase for systems under construction:

- Clear debris and secure loose materials in and around arrays to avoid wind-blown objects that can damage modules.
- Make sure all exposed connectors are capped or—at a minimum—fastened under the modules, where their exposure to water and dust ingress is minimized.
- Secure cables to the racking to avoid abrasion and stress from wind loading.

Pre-storm phase for commissioned systems:

- Conduct a torque audit on all fasteners.
- Stow single-axis tracker systems per manufacturer specifications.
- Power down all components by opening breakers, fuses, and switches.

Post-storm phase for systems under construction (in addition to the recommendations for commissioned systems):

- Inspect racking posts for shifting or loosening that may have been caused by erosion.
- Document any flooding of open trenches and exposed cables.
- Check integrity of module pallets.
- Replace any open, unmated, connectors that appear to be dirty or wet.

Post-storm phase for commissioned systems:

- Visually inspect damages to PV modules (front and back), mounting structures, fasteners, cables, connectors (module-to-module and homerun), combiner boxes, inverter boxes, wiring, and other components. It is important to 1) check purlins and rails for evidence of cracks or deformation; 2) look for evidence of cable abrasion; 3) replace broken zip ties and other failed cable fasteners; and 4) verify that connectors are not sitting in pooled water or show evidence of submersion (e.g., algal growth).
- Dry and clean the interiors of combiner boxes and inverter boxes. Components inboxes that were exposed to water or high humidity should be closely inspected for indicators of moisture ingress, replaced if necessary, and thereafter monitored for evidence of increased resistance to ensure electrical safety.

Open Access Journal of Climate Change
Research and Reviews
ISSN 2637-8078 | Volume 1 - Issue 1 - 2022

Article
Received: 20 Jan 2022
Accepted: 28 Jan 2022
Published: 02 Feb 2022

Author(s)
Ole Rössler*
Author Affiliations
Institute of Climate and Water, Bern University, Switzerland
*Corresponding author: Ole Rössler, Institute of Climate and Water, Bern University, Switzerland.

Cite this article
Rössler O. Storm Kyrill and the storms of mid-January 2007: Societal and Energy Impacts in Europe. Open Access J Clim Change Res Rev. 2022; 1(1): 1-7. DOI: 10.54026/OACCRR/1000005

Storm Kyrill and the storms of mid-January 2007: Societal and Energy Impacts in Europe

Abstract

January 2007 was a stormy period in Europe with impacts on societal infrastructure and implications for energy technology. A series of storms hit the continent with the most severe storm being Storm Kyrill which crossed Ireland, the United Kingdom, and the north of Europe. Storms Kyrill and Lothar (1999) rank the most important of these for the infrastructure damage. It is noted that Kyrill has figures quasi-stationary blocked anticyclones in recent history. The storm spawned a high intensity derecho that produced extreme wind speeds and damage in Germany. Storm Kyrill was the most expensive storm in Germany's insurance history and the most costly natural disaster in Germany's history. The storm caused widespread disruption of transport and communication networks and caused power outages affecting millions of people. The storm also caused damage to the continental European grid for the year, in some cases exceed legislating Storm Kyrill. This contributed a premium in Nordpool electricity prices and caused a shortfall in Germany's PV production. The storm also contributed to a rapid increase in natural gas prices. Storm Kyrill's impact on the electricity and gas infrastructure compared around Storm Lothar. The weak wind infrastructure, coupled with shipping accidents and offshore incidents in severe possible risks. Unusually large waves have been registered at the FINO platforms in the German Bight. Storm Kyrill's impact on the electricity and gas infrastructure compared around Storm Lothar. The weak wind infrastructure, coupled with shipping accidents and offshore incidents in severe possible risks. Unusually large waves have been registered at the FINO platforms in the German Bight. Storm Kyrill's impact on the electricity and gas infrastructure compared around Storm Lothar. The weak wind infrastructure, coupled with shipping accidents and offshore incidents in severe possible risks. Unusually large waves have been registered at the FINO platforms in the German Bight.

Keywords
Storm Kyrill, Storm Lothar, Storm Jeanett, Storm Cyntia, Storm Erwin, Storm Gudrun, Storm Kirsten, Storm Emma, Storm Joachim, Storm Paul, Storm Quintus, Storm Tilo, Storm Wiebke, Storm Daniela, Storm Emil, Storm Frederic, Storm Gero, Storm Hans, Storm Ingo, Storm Jonas, Storm Karl, Storm Leo, Storm Martin, Storm Norbert, Storm Olaf, Storm Petra, Storm Quenton, Storm Ralf, Storm Susanne, Storm Tilo, Storm Uwe, Storm Vera, Storm Wolfgang, Storm Xaver, Storm Yvonne, Storm Zeynep, Storm Ulrike, Storm Christian, Storm Dirk, Storm Elke, Storm Frank, Storm Gero, Storm Hartmut, Storm Ingo, Storm Jan, Storm Kai, Storm Lars, Storm Mareike, Storm Nina, Storm Oliver, Storm Petra, Storm Quirin, Storm Ralf, Storm Sabine, Storm Tobias, Storm Ulrike, Storm Volker

Supplement

The supplement related to this article is available online at: https://doi.org/10.5194/adgeo-58-135-2023-supplement.

Competing interests

The author has declared that there are no competing interests.

Disclaimer

Publisher's note: Copernicus Publications remains neutral with regard to jurisdictional claims in published maps and institutional affiliations.

Special issue statement

This article is part of the special issue "European Geosciences Union General Assembly 2022, EGU Division Energy, Resources & Environment (ERE)". It is a result of the EGU General Assembly 2022, Vienna, Austria, 23–27 May 2022.

Acknowledgements

The author gratefully acknowledges data from national tide gauge networks of the UK, Belgium, the Netherlands, Germany, Denmark, and Norway. The tide gauge data for the UK, Belgium, the Netherlands, Denmark, and Norway was downloaded from Internet servers. For the UK, Victoria Grobler (Environment Agency) emailed data for one additional tide gauge at Southend. For Germany, Wilfried Wiechmann of the Bundesanstalt für Gewässerkunde kindly provided tide gauge data by email. Bjørn Frederiksen of Kystdirektoratet also emailed data for three tide gauge stations in northern Denmark that were not provided on the public Internet server. Gerda van Vliet provided information on rescues by the Koninklijke Nederlandse Redding Maatschappij (KNRM, the Dutch lifeboat service) along the Netherlands coast. The following people provided background reports, data, or other information to support this review: Maria Bluemel and Theide Wöffler (Landesbetrieb für Küstenschutz, Nationalpark, und Meeresschutz Schleswig-Holstein, Germany), Christoph Gatzen (Free University of Berlin, Germany), Edwin Granneman (Kustwacht, the Netherlands), Polly Hadziabdic (British Oceanographic Data Centre, UK), Ivan Haigh (National Oceanography Centre, University of Southampton, UK), Julia Lockwood (Met Office Hydrographic Office, UK), Delila Montes (International Energy Agency), Irene Perez-Gonzalez (Bundesamt für Seeschifffahrt und Hydrographie, Germany), Reidun Gangsta Skaland (Met.no, Norway), and Annette Zijderfeld (Rijkswaterstaat, the Netherlands). The manuscript benefitted from the comments and suggestions of two reviewers, the editor (Gregor Giebel), and the copy editor (Viola Zierenberg).

Review statement

This paper was edited by Gregor Giebel and reviewed by two anonymous referees.

References

AON Benfield: Historie von 1703 bis 2012: Winterstürme in Europa, Stand: Januar 2013, AON Benfield, 2013.

BBC: Huge storms sweep northern Europe, http://news.bbc.co.uk/2/hi/europe/6274377.stm (last access: 10 January 2023), 18 January 2007.

Behrens, A. and Günther, H.: Operational wave prediction of extreme storms in Northern Europe, Nat. Hazards, 49, 387–399, 2009.

Bradshaw, E.: Annual Report for 2007 for the UK National Tide Gauge Network and Related Sea Level Science, National Tide and Sea Level Facility, NERC 10001897, 2007.

Bradshaw, E., Woodworth, P. L., Hibbert, A., Bradley, L. J., Pugh, D. T., Fane, C., and Bingley, R. M.: A century of sea level measurements at Newlyn, Southwest England, Mar. Geod., 39, 115–140, 2016.

Brugge, R.: British Isles weather diary, https://www.met.reading.ac.uk/~brugge/diary2007.html#200701 (last access: 10 January 2023), January 2007.

Caithness Windfarm: Detailed accidents to 19 June 2018, Wind turbine accident compilation, updated regularly, https://scotlandagainstspin.org/wp-content/uploads/2023/01/Detailed-incidents-to-31-Dec2022.pdf (last access: 10 January 2023), 30 July 2018.

Christou, M. and Ewans, K.: Examining a comprehensive dataset containing thousands of freak wave events. Part 1 – Description of the data and quality control procedure, Proceedings of the ASME 2011 30th International Conference on Ocean, Offshore and Arctic Engineering, OMAE2011, 19–24 June 2011, Rotterdam, the Netherlands, OMAE2011-50168, 2011.

Deutsche Rückversicherung Aktiengesellschaft: Sturmdokumentation 2007 Deutschland, edited by: Axer, T., Bistry, T., Müller, M., Reiner, A., and Süsser, M., 38 pp., Deutsche Rückversicherung Aktiengesellschaft, Düsseldorf, Berlin, https://www.deutschereuck.de/fileadmin/Downloads/Sturmdoku_2007_web.pdf (last access: 10 January 2023), 2007.

Diamond, K. E.: Extreme weather impacts on offshore wind turbines: Lessons learned, Nat. Resour. Env., 27, 1–5, 2012.

Ditlevsen, C., Ramos, M. M., Sørensen, C., Ciocan, U. R., and Pionkowitz, T.: Højvandsstatistikker 2017, Miljø- og Fødevareministeriet, Kystdirektoratet Lemvig, https://www.kyst.dk/media/80372/hoejvandsstatistikker2017revideret110220l9.pdf (last access: 10 January 2023), February 2018.

Donat, M. G., Pardowitz, T., Leckebusch, G. C., Ulbrich, U., and Burghoff, O.: High-resolution refinement of a storm loss model and estimation of return periods of loss-intensive storms over Germany, Nat. Hazards Earth Syst. Sci., 11, 2821–2833, [redacted], 2011.

Dotzek, N., Emeis, S., Lefevre, C., and Gerpott, J.: Waterspouts over the North and Baltic Seas: Observations and climatology, prediction and reporting, Meteorol. Z., 19, 115–129, 2010.

DW: Killer winds in Europe expected to cause heavy financial loss, https://www.dw.com/en/killer-winds-in-europe-expected-to-cause-heavy-financial-loss/a-2317752 (last access: 10 January 2023), 18 January 2007a.

DW: Power cuts in Europe as continent begins to clean up, https://www.dw.com/en/power-cuts-in-europe-as-continent-begins-clean-up/a-2319624 (last access: 10 January 2023), 20 January 2007b.

DWD: Klimatologische Bewertung der jüngsten Starkwindereignisse (ANATOL und LOTHAR) aus der Sicht der Klimatologie der freien Atmosphäre, 8 pp., https://www.dwd.de/DE/leistungen/besonderereignisse/sturm/e/20000201_bewertung_lothar-anatol.html (last access: 10 January 2023), 2000.

DWD: 18. Januar 2007: Windfeld von Kyrill über Deutschland, Rückblick auf einen der bisher schwersten Orkane, Pressemitteilung, Deutscher Wetterdienst, Offenbach, 16 Januar 2012.

Emeis, S. and Türk, M.: Wind-driven wave heights in the German Bight, Ocean Dynam., 59, 463–475, 2009.

Environment Agency: Thames Barrier Project Pack 2018, Environment Agency, Thames Barrier View Cafe and Information Centre, London, available upon request, email: thamesbarrierenquiries@environment-agency.gov.uk, January 2018.

Fink, A. H., Brücher, T., Ermert, V., Krüger, A., and Pinto, J. G.: The European storm Kyrill in January 2007: synoptic evolution, meteorological impacts and some considerations with respect to climate change, Nat. Hazards Earth Syst. Sci., 9, 405–423, [redacted], 2009.

Gardiner, B.: Appendix 3: Background information on 11 storms selected for detailed analysis, European Forest Institute, Atlantic European Regional Office – EFIAtlantic, 161 pp., https://ec.europa.eu/environment/forests/pdf/Final_Report_Appendix_3.pdf (last access: 10 January 2023), 23 July 2010.

Gatzen, C., Pucik, T., and Ryva, D.: Two cold-season derechoes in Europe, Atmos. Res., 100, 740–748, 2011.

Gönnert, G., Isert, K., Giese, H., and Plüss, A.: Charakterisierung der Tidekurve, Die Küste, 68, 99–141, 2004.

Jensen, J. and Müller-Navarra, S. H.: Storm surges on the German coast, Die Küste, 74, 92–124, 2008.

Kettle, A. J.: The North Sea surge of 31 October–1 November 2006 during Storm Britta, Adv. Geosci., 45, 273–279, [redacted], 2018.

Kettle, A. J.: Storm Tilo over Europe in November 2007: storm surge and impacts on societal and energy infrastructure, Adv. Geosci., 49, 187–196, [redacted], 2019.

Kettle, A. J.: Storm Xaver over Europe in December 2013: Overview of energy impacts and North Sea events, Adv. Geosci., 54, 137–147, [redacted], 2020.

Kettle, A. J.: Storm Anatol over Europe in December 1999: impacts on societal and energy infrastructure, Adv. Geosci., 56, 141–153, [redacted], 2021.

KNMI: Nieuwsbericht, De zware storm Kyrill van 18 januari 2007, https://www.knmi.nl/over-het-knmi/nieuws/de-zware-storm-kyrill-van-18-januari-2007 (last access: 10 January 2023), 17 January 2007.

Kvamme, D.: Ekstremvær nr.1/2007 – "Per", Intern Rapport, 15 pp., Meteorogisk Institutt met.no, Bergen, 14 February 2007.

Kvendseth, S. S.: Giant Discovery, a history of Ekofisk through the first 20 years, Phillips Petroleum Company Norway, https://www.nb.no/items/URN:NBN:no-nb_digibok_2019090248002?page=5 (last access: 10 January 2023), 1988.

Larsén, X. G., Du, J., Bolanos, R., and Larsen, S.: On the impact of wind on the development of wave field during storm Britta, Ocean Dynam., 67, 1407–1427, 2017.

Lloyds Casualty Week: 26Jan2007, Lloyd's MIU, Telephone House, London, https://dione.lib.unipi.gr/xmlui/bitstream/handle/unipi/1916/Casualty_Week_Jan_26_2.pdf?sequence=3&isAllowed=2 (last access: 10 January 2023), 2007a.

Lloyds Casualty Week: 02Feb2007, Lloyd's MIU, Telephone House, London, https://dione.lib.unipi.gr/xmlui/bitstream/handle/unipi/1902/Casualty_Week_Feb_2_2.pdf?sequence=3&isAllowed=2 (last access: 10 January 2023), 2007b.

Ma, Y., Martinez-Vazquez, P., and Baniotopoulos, C.: Wind turbine collapse cases: a historical overview, Institution of Civil Engineers, Proceedings, Structures and Buildings, 172, 547–555, [redacted]17.00167, 2018.

Magnusson, A. K.: What is true sea state? Proceedings of the 11th International Workshop on Wave Hindcasting and Forecasting and Coastal Hazard Symposium, JCOMM Halifax, Canada, 18–23 October 2009, Technical Report No. 52, WMO/TD-No. 1533, IOC Workshop Report No. 232, 2009.

Magnusson, A. K., Johannessen, J., Dagestad, K.-F., Breivik, O., Aarnes, O. J., and Furevik, B.: Bølge-strøm interaksjon til nytte for oljeindustri, WACUSAR_sluttrapport.doc, NERSC, met.no, 19 December 2008.

MAIB: Report on the investigation of the structural failure of MSC Napoli English Channel on 18 January 2007, Marine Accident Investigation Branch, Southampton, UK, Report No. 9/2008, April 2008.

Met Eireann: Monthly Weather Bulletin, No. 240 [redacted] (last access: 10 January 2023), January 2007.

Monserrat, S., Vilibić, I., and Rabinovich, A. B.: Meteotsunamis: atmospherically induced destructive ocean waves in the tsunami frequency band, Nat. Hazards Earth Syst. Sci., 6, 1035–1051, [redacted] 2006.

Müller-Westermeier, G.: Beschreibung und klimatologische Bewertung des Orkantiefs "Kyrill", Deutscher Wetterdienst – Nationale Klimaüberwachung, https://www.dwd.de/DE/leistungen/besondereereignisse/sturme/20070118_orkan_kyrill.html (last access: 10 January 2023), 26 January 2007.

Neumann, T.: FINO and the mast shadow effect, 52nd IEA Topical Expert Meeting, Wind and wave measurements at offshore locations, Berlin, Germany, organized by TU Berlin and Germanischer Lloyd, International Energy Agency, Implementing Agreement for Co-operation in the Research, Development and Deployment of Wind Turbine Systems, Task 11, February 2007.

Neumann, T. and Nolopp, K.: Three years of operation of far offshore measurements at FINO1, DEWI Magazine, 30, 42–46, 2007.

NLWKN: Sturmflut am 12. Januar 2007: Nordseeküste kam glimpflich davon 12. Januar 2007 (aktualisiert am 15. Januar 2007): Dünenabbrüche auf den ostfriesischen inseln, https://www.nlwkn.niedersachsen.de/startseite/aktuelles/presse_und_offentlichkeitsarbeit/pressemitteilungen/-41838.html (last access: 10 January 2023), 15 January 2007a.

NLWKN: Sturmflut von 19. Januar: Es kam nicht so schlimm wie befürchtet. 19. Januar 2007: keine Dünenabbrüche auf den Inseln!Für das Wochenende wird erhöhtes tidewasser erwartet, https://www.nlwkn.niedersachsen.de/startseite/aktuelles/presse_und_offentlichkeitsarbeit/pressemitteilungen/-41867.html (last access: 10 January 2023), 22 January 2007b.

Pattiaratchi, C. B. and Wijeratne, E. M. S.: Are meteotsunamis an underrated hazard?, Philos. T. R. Soc. A, 373, 2140377, [redacted], 2015.

Petroleum Safety Authority Norway: Petroleum Safety Authority Norway Annual Report 2006, Supervision and Facts, Stavanger, 26 April 2007.

Petroliagis, T. I. and Pinson, P.: Early warnings of extreme winds using the ECMWF Extreme Forecast Index, Meteorol. Appl., 21, 171–185, 2014.

Pinto, J. G., Gomara, I., Masato, G., Dacre, H. F., Woolings, T., and Caballero, R.: Large-scale dynamics associated with clustering of extratropical cyclones affecting Western Europe, J. Geophys. Res.-Atmos., 119, 13704–13719, 2014.

Pleskachevsky, A. L., Lehner, S., and Rosenthal, W.: Storm observations by remote sensing and influences of gustiness on ocean waves and on generation of rogue waves, Ocean Dynam., 62, 1335–1351, 2012.

Pugh, D. T.: Tides, Surges and Mean Sea Level, John Wiley and Sons, https://eprints.soton.ac.uk/19157/1/sea-level.pdf (last access: 10 January 2023), 1987.

Roberts, J. F., Champion, A. J., Dawkins, L. C., Hodges, K. I., Shaffrey, L. C., Stephenson, D. B., Stringer, M. A., Thornton, H. E., and Youngman, B. D.: The XWS open access catalogue of extreme European windstorms from 1979 to 2012, Nat. Hazards Earth Syst. Sci., 14, 2487–2501, https://doi.org/10.5194/nhess-14-2487-2014, 2014.

Rose, S., Jaramillo, P., Small, M. J., Grossmann, I., and Apt, J.: Quantifying the hurricane risk to offshore wind turbines, P. Natl. Acad. Sci. USA, 109, 3247–3252, 2012.

Rosenorn, A. S.: Vintervejret 2006–2007, Vejret, 111, 28–31, 2007.

Rosenthal, W., Pleskachevsky, A. L., Lehner, S., and Brusch, S.: Observation and modeling of high individual ocean waves and wave groups caused by a variable wind field, 12th International Workshop on Wave Hindcasting and Forecasting, 30 October–4 November 2011, Kohala Coast, Hawai'i, HI, [redacted] (last access: 10 January 2023), 2011.

RWS: Verslag van de stormvloed van 31 oktober en 1 november 2006 (SR84), Ministerie van Veerkeer en Waterstaat, Rijkswaterstaat, Stormvloedwaarschuwingsdienst/SVSD, Postbus 20907, 2500 EX's-Gravenhage, https://waterberichtgeving.rws.nl/water-en-weer/verwachtingen-water/water-en-weerverwachtingen-waternoordzee/stormvloedrapportages/stormvloedverslagen (last access: 10 January 2023), November 2006.

RWS: Verslag van de stormvloed van 18 en 19 januari 2007 (SR86), Ministerie van Verkeer en Waterstaat, Rijkswaterstaat, Stormvloedwaarschuwingsdienst/SVSD, Postbus 20907, 2500 EX's-Gravenhage, [redacted] (last access: 10 January 2023), January 2007.

SMHI: Per – Januarstormen 2007, https://www.smhi.se/kunskapsbanken/meteorologi/per-januaristormen-2007-1.5287 (last access: 10 January 2023), 6 August 2009.

Sørensen, C., Ingvardsen, S. M., Andersen, I., and Kloster, B. B.: Højvandsstatistikker 2007, Extreme sea level statistics for Denmark, 2007, Kystdirektoratet, https://kyst.dk/media/80365/00_hojvandsstatistik_2007-1-1-1.pdf (last access: 10 January 2023), December 2007.

Statistica: The costliest winter storms ever to hit Europe, Fatalities and financial losses of Europe's 10 costliest winter storms (source Munich Re), https://www.statista.com/chart/4147/the-costliest-winter-storms-ever-to-hit-europe/ (last access: 10 January 2023), 8 December 2015.

Stull, R. B.: An Introduction to Boundary Layer Meteorology, Kluwer Academic Publishers, Dordrecht, https://link.springer.com/book/10.1007/978-94-009-3027-8 (last access: 10 January 2023), 1988.

Tetzlaff, G.: Der Orkan Kyrill, Info, DKKV Deutsches Komitee Katastrophenvorsorge e.V., 1–2, Februar/März 2007, No. 1+2, https://dkkv.org/uploads/media/InfoBlatt1u2_07.pdf (last access: 10 January 2023), 2007.

Wikipedia: Cyclone Kyrill, https://en.wikipedia.org/wiki/Cyclone_Kyrill, last access: 22 March 2022.

XWS: Extreme Wind Storms Catalogue, http://www.europeanwindstorms.org/cgi-bin/storms/storms.cgi, last access: 10 January 2023.

Advances in Geosciences
An open-access journal for refereed proceedings and special publications

All site content, except where otherwise noted, is licensed under the Creative Commons Attribution 4.0 License.